Received: 5 March 2022 | Revised: 6 May 2022 | Accepted: 11 May 2022
DOI: 10.1002/glia.24220

GLIA
WILEY

RESEARCH ARTICLE

Transforming growth factor-beta signaling modulates perineurial glial bridging following peripheral spinal motor nerve injury in zebrafish

Kimberly A. Arena[1,2] | Yunlu Zhu[1] | Sarah Kucenas[1,2]

[1]Department of Biology, University of Virginia, Charlottesville, Virginia, USA

[2]Program in Fundamental Neuroscience, University of Virginia, Charlottesville, Virginia, USA

Correspondence
Sarah Kucenas, Department of Biology, University of Virginia, Physical and Life Sciences Building, Rm 312, PO Box 400328, Charlottesville, VA 22904-4328, USA.
Email: sk4ub@virginia.edu

Funding information
Jefferson Scholars Foundation; National Institute of General Medical Sciences, Grant/Award Number: T32GM008136; National Institute of Neurological Disorders and Stroke, Grant/Award Number: NS107525; National Institutes of Health

Abstract

Spinal motor nerves are necessary for organismal locomotion and survival. In zebrafish and most vertebrates, these peripheral nervous system structures are composed of bundles of axons that naturally regenerate following injury. However, the cellular and molecular mechanisms that mediate this process are still only partially understood. Perineurial glia, which form a component of the blood-nerve barrier, are necessary for the earliest regenerative steps by establishing a glial bridge across the injury site as well as phagocytosing debris. Without perineurial glial bridging, regeneration is impaired. In addition to perineurial glia, Schwann cells, the cells that ensheath and myelinate axons within the nerve, are essential for debris clearance and axon guidance. In the absence of Schwann cells, perineurial glia exhibit perturbed bridging, demonstrating that these two cell types communicate during the injury response. While the presence and importance of perineurial glial bridging is known, the molecular mechanisms that underlie this process remain a mystery. Understanding the cellular and molecular interactions that drive perineurial glial bridging is crucial to unlocking the mechanisms underlying successful motor nerve regeneration. Using laser axotomy and in vivo imaging in zebrafish, we show that transforming growth factor-beta (TGFβ) signaling modulates perineurial glial bridging. Further, we identify connective tissue growth factor-a (*ctgfa*) as a downstream effector of TGF-β signaling that works in a positive feedback loop to mediate perineurial glial bridging. Together, these studies present a new signaling pathway involved in the perineurial glial injury response and further characterize the dynamics of the perineurial glial bridge.

KEYWORDS
motor nerve, perineurial glia, regeneration, TGFβ, zebrafish

1 | INTRODUCTION

Motor nerves, the peripheral nerves that control locomotion, require perineurial glia, the protective barrier of the nerve, and Schwann cells, peripheral myelinating cells, for development (Binari et al., 2013; Clark et al., 2014; Jessen et al., 2015; Kucenas, 2015; Kucenas, Takada, et al., 2008). Following axonal projection from the central nervous system (CNS) through motor exit point transition zones into the

peripheral nervous system (PNS), individual neural crest-derived Schwann cell precursors hone towards axons in the periphery, associate with them in a 1:1 ratio, and differentiate into myelinating Schwann cells (D'Rozario et al., 2017; Jessen et al., 2015; Jessen & Mirsky, 2005). In zebrafish and mice, the perineurium, made of floor plate-derived perineurial glia, ensheaths these axon-Schwann cell bundles into fascicles, protecting the nerve by establishing a component of the blood-nerve-barrier (Clark et al., 2014; Kucenas, 2015; Peltonen et al., 2013). Perturbation to perineurial glial migration into the periphery adversely affects Schwann cell development and differentiation (Binari et al., 2013). Reciprocally, perturbing Schwann cell development prevents or delays perineurial glial migration into the periphery (Morris et al., 2017). In the absence of perineurial glia, motor axons exit the spinal cord ectopically and Schwann cells fail to ensheath motor nerves (Kucenas, Takada, et al., 2008). Similarly, in *colorless* zebrafish mutants, which lack Schwann cells due to a mutation in *sox10*, perineurial glial migration into the periphery is delayed and these cells fail to properly ensheath motor nerves (Lewis & Kucenas, 2014). Therefore, reciprocal cellular and molecular interactions between Schwann cells and perineurial glia during development are essential for motor nerve development. These same glial cells that are crucial for spinal motor nerve development play essential cellular and molecular roles in modulating regenerative responses after nerve injury to drive successful and effective regeneration (Cattin & Lloyd, 2016; Gonzalez & Allende, 2021; Jessen & Mirsky, 2019; Lewis & Kucenas, 2014).

Immediately following peripheral motor nerve injury, axons experience acute axonal degeneration, where the proximal and distal stumps of the nerve degenerate away from the injury site. The distal stump then undergoes Wallerian degeneration, a highly conserved pattern of anterograde degeneration of both the axon and associated myelin sheaths, resulting in rapid fragmentation of the axon (Coleman & Freeman, 2010; Lewis & Kucenas, 2014; Villegas et al., 2012; Waller, 1850). Axonal and myelin debris is then removed by macrophages, Schwann cells, and perineurial glia, establishing a growth permissive environment (Cattin & Lloyd, 2016; Huebner & Strittmatter, 2009; Lewis & Kucenas, 2014; Waller, 1850).

The perineurium has long been suspected to play an active role in motor nerve regeneration (Behrman & Acland, 1981; Popović et al., 1994; Schröder et al., 1993). Previous studies from our lab discovered that following spinal motor nerve injury in zebrafish, perineurial glia clear debris and form a glial bridge across the injury site that is essential for regeneration, and this process precedes Schwann cell infiltration into the injury site (Lewis & Kucenas, 2014). As axons degenerate and perineurial glia begin to bridge, Schwann cells convert into distinct repair (Bungner) Schwann cells. Schwann cell function switches from myelination of axons to phagocytosis of myelin and axonal debris as well as collective migration, forming Bands of Bungner that guide regenerating axons across the injury site. Following regeneration, Schwann cells begin to re-myelinate the newly established axons (Brosius Lutz et al., 2022; Fernandez et al., 2017; Jessen & Mirsky, 2019; Parrinello et al., 2010; Webber & Zochodne, 2010). Together, Schwann cells and perineurial glia provide essential physical structures that are necessary for proper motor nerve regeneration. Though many studies have explored the Schwann cell injury response (Brosius Lutz et al., 2022; Clements et al., 2017; K. R. Jessen & Mirsky, 2016; Allison F. Rosenberg et al., 2014; Schira et al., 2018), the cellular and molecular mechanisms that drive perineurial glial behaviors essential for motor nerve regeneration remain unknown.

Transforming growth factor beta-1 (TGFβ-1) is an important regulator of regenerative processes (Abarca-Buis et al., 2021; Katsuno & Derynck, 2021; Sulaiman & Nguyen, 2016). In particular, Schwann cells both secrete TGFβ-1 following peripheral nerve injury to enhance debris clearance and suppress fibroblast proliferation (Schira et al., 2018; Sulaiman & Nguyen, 2016) as well as require TGFβ signaling to successfully migrate across the injury site (Clements et al., 2017). Therefore, TGFβ signaling is crucial for Schwann cell reprogramming, debris clearance, and subsequent nerve regeneration. Connective tissue growth factor (CTGF) is another secreted protein involved in angiogenesis and wound healing (Mokalled et al., 2016; Mukherjee et al., 2021). CTGF directly binds TGFβ-1 and enhances receptor binding, working in a positive feedback loop to drive TGFβ signaling. At low TGFβ-1 concentrations, CTGF even potentiates the phosphorylation of Smad2 induced by TGFβ-1 (Abarca-Buis et al., 2021; Abreu et al., 2002). Previous studies demonstrate that CTGF is actively involved in regenerative processes including driving glial bridging after spinal cord injury (Mokalled et al., 2016) and modulating TGFβ/pSmad3 signaling to promote cardiac regeneration (Mukherjee et al., 2021). Additionally, CTGF is secreted by Schwann cells following peripheral nerve injury (Schira et al., 2018). Therefore, CTGF is an important regulator of TGFβ signaling and cellular responses following injury. Though crucial roles of both TGFβ-1 and CTGF in regeneration are known, it remains unknown how these signals might be affecting perineurial glial responses following peripheral motor nerve injury.

While peripheral motor nerves possess regenerative capabilities, regaining full function following injury is extremely limited in humans. Currently, less than 10% of peripheral nerve injury patients achieve full functional recovery (Lopes et al., 2022; Witzel et al., 2005; Zochodne, 2012) with patients commonly facing lifelong functional impairment and neuropathic pain (Balakrishnan et al., 2021; Lopes et al., 2022; Menorca et al., 2013). Understanding the cellular and molecular mechanisms between glial cells and the molecular drivers of their regenerative processes is crucial for developing new targeted therapies to enhance regenerative capacity.

Here, we identify a signaling pathway that drives perineurial glial bridging, an essential regenerative process, after spinal motor nerve injury. We demonstrate that TGFβ signaling modulates perineurial glial dynamics after injury by initiating bridging behaviors. We then show that connective tissue growth factor a (*ctgfa*), a component of this signaling cascade, is also required for perineurial glial bridging. Together, these studies present TGFβ signaling as a driver of perineurial glial bridging, a process that is

crucial for successful and functional motor nerve regeneration. Elucidating the cellular and molecular mechanisms that regulate perineurial glial behaviors following injury is crucial to further understanding successful motor nerve regeneration.

2 | MATERIALS AND METHODS

2.1 | Fish husbandry

All animal studies were approved by the University of Virginia Institutional Animal Care and Use Committee. Zebrafish strains used in this study include: AB*, *Tg(nkx2.2a:megfp)*^{vu17} (Kirby et al., 2006; Kucenas, Snell, & Appel, 2008), *Tg(olig2:dsred2)*^{vu19} (Kucenas, Snell, & Appel, 2008), *Tg(nkx2.2a(-3.5):nls-egfp)*^{uva1} (Fontenas & Kucenas, 2021), *Tg(nkx2.2a(-3.5):nls-mcherry)*^{uva2} (Zhu et al., 2019), *Tg(sox10(-7.2):megfp)*^{sl3} (Kirby et al., 2006), *Tg(mpeg1:egfp)*^{gl22} (Ellett et al., 2011), *Tg(sox10:gal4-VP16;UAS-E1B:NTR-mcherry)*^{el159} (Das & Crump, 2012); *Tg(nkx2.2a:gal4-VP16;UAS:NTR-mcherry)*^{uva4} (this article), *Tg(ctgfa:egfp)*^{pd96} (Mokalled et al., 2016), and *ctgfa*^{bns50} (Mokalled et al., 2016) (Table 1). Embryos were produced by pairwise natural matings, raised at 28.5°C in egg water, staged according to hours or days post fertilization (hpf or dpf, respectively), and screened for correct fluorescence of transgenic lines. Embryos of either sex were used for all experiments (Kimmel et al., 1995). Embryos used for microscopy or immunohistochemistry were treated at 24 hpf with 0.003% phenylthiourea (PTU) in egg water to reduce development of pigmentation.

TABLE 1 Zebrafish lines used in this study and their genotypes

Full name	Abbreviation	Reference
AB*	AB*	
Tg(nkx2.2a:megfp)^{vu17}	*nkx2.2a:megfp*	Kirby et al. (2006); Kucenas, Snell, and Appel (2008)
Tg(olig2:dsred2)^{vu19}	*olig2:dsred*	Kucenas, Snell, and Appel (2008)
Tg(nkx2.2a(-3.5):nls-egfp)^{uva1}	*nkx2.2a:nls-egfp*	Fontenas and Kucenas (2021)
Tg(nkx2.2a(-3.5):nls-mcherry)^{uva2}	*nkx2.2a:nls-mch*	Zhu et al. (2019)
Tg(sox10(-7.2):megfp)^{sl3}	*sox10:megfp*	Smith et al. (2014)
Tg(mpeg1:egfp)^{gl22}	*mpeg1:egfp*	Ellett et al. (2011)
Tg(nkx2.2a(-3.5):gal4-VP16;UAS-E1B:NTR-mcherry)^{uva4}	*nkx2.2a:gal4; UAS:NTR-mch*	This article
Tg(sox10:gal4-VP16;UAS-E1B:NTR-mcherry)^{el159}	*sox10:gal4; UAS:NTR-mch*	Das and Crump (2012)
Tg(ctgfa:egfp)^{pd96}	*ctgfa:egfp*	Mokalled et al. (2016)
ctgfa^{bns50}	*ctgfa*	Mokalled et al. (2016)

2.2 | Generation of transgenic lines

All constructs were created using the Tol2kit Gateway-based cloning system (Kwan et al., 2007). Vectors p5E-nkx2.2a(-3.5) (Pauls et al., 2007), pME-Gal4-VP16, and p3E-polyA, were inserted into a pDesTol2CG2 destination vector through an LR reaction (Kwan et al., 2007). Final constructs were amplified and sequenced to confirm correct insertion. To generate a stable transgenic line, plasmid DNA was microinjected at a concentration of 20 ng/μl in combination with 100 ng/μl *Tol2* transposase mRNA into embryos at the one-cell stage. Injected embryos were then screened for founders (Kawakami, 2004). To generate the *Tg(nkx2.2a:gal4-VP16;UAS:NTR-mcherry)* line, *UAS:NTR-mcherry* plasmid DNA was microinjected at a concentration of 20 ng/μl in combination with 100 ng/μl *Tol2* transposase mRNA into *Tg(nkx2.2a:gal4-VP16;cmlc2:egfp)*^{uva4} embryos at the one-cell stage. Injected embryos were then screened for founders (Kawakami, 2004).

2.3 | In vivo imaging

At 24 hpf, all embryos used for imaging were treated with 0.003% PTU to reduce pigment formation. Embryos were screened for correct fluorescence and manually dechorionated. At specified stages, embryos and larvae were anesthetized using 3-aminobenzoic acid esther (Tricaine) and mounted in 0.8% low-gelling point agarose in 4-well glass bottom 35 mm Petri dishes (Fisher, Greiner Bio-One). Following mounting, Petri dishes were filled with egg water containing Tricaine. In vivo imaging was conducted on a motorized Zeiss AxioObserver Z1 microscope equipped with Quorum WaveFX-XI (Quorum Technologies) or Andor CSU-W (Andor Oxford Instruments Plc.) spinning disk confocal system. A 40X water objective (NA = 1.1) was used to capture all images and time-lapses. Time-lapses were set to image in 5-minute intervals for 6–12 h, depending on the experiment. For experiments using *ctgfa*^{bns50} larvae, time-lapses were set to image in 2-h intervals for 10 h. *Z* stacks of 1–2 μm were collected for each image in a time-lapse. Image processing and limited adjustments were made using MetaMorph software and FIJI (ImageJ).

2.4 | Nerve transection

Nerve transections were preformed using a nitrogen-dye (435 nm) pumped MicroPoint laser (Andor technology) connected to a spinning disk confocal system (Quorum Technologies) controlled by MetaMorph as previously published (Lewis & Kucenas, 2014; Gwendolyn M. Lewis & Kucenas, 2013; Morris et al., 2017; Rosenberg et al., 2012). Injuries were conducted using either a 40X water (NA = 1.1) or 63X water (NA = 0.8) objective. Ablation power ranged from 40 to 60 depending on the size of the nerve, the mounting of the larvae, the age of the larvae, and the age of the nitrogen-dye. For all experiments, injuries were induced in 1–3 spinal motor nerves within hemisegments 4–16, creating an approximately 10 μm injury. Nerves with injuries larger than 10 μm or without a full

transection were not included in analyses. To transect nerves, an ellipse was virtually drawn around the desired injury site on an image of the nerve in MetaMorph. The laser was pulsed within the designated region of interest (ROI) until the nerve was injured. Injuries were confirmed by presence of axonal debris and lack of return of motor neuron fluorescence in the ROI after 20 s. In vivo imaging of transected nerves was conducted as described above. In fish that were fixed for antibody staining following nerve transection, the first 10 nerves in each fish were injured.

2.5 | Drug treatments

The following drug treatments were performed in 24-well plates with up to five larvae per well:

2.6 | TGFβ inhibition

Larvae were incubated in either 1.5 ml of 10 μM SB431542 (Morris et al., 2017; Sun et al., 2006), a selective inhibitor of the TGFβ receptor-I, in 1% DMSO in PTU water or 1.5 ml of 1% DMSO in PTU water at 28.5°C in dark conditions. Larvae were treated with either drug or control DMSO solutions beginning at 4 dpf and placed in an incubator in dark conditions at 28.5°C for approximately 24 h. Fresh drug or DMSO solutions were replaced at 5 dpf and larvae were placed back in the 28.5°C incubator in dark conditions for an additional 24 h. At 6 dpf, larvae were treated with fresh drug or DMSO solutions and mounted for imaging. Tricaine was added to drug or DMSO solutions for imaging, and larvae were submerged in these solutions for the entirety of imaging.

2.7 | Ronidazole treatment

Larvae were incubated at 5 or 6 dpf in either 1.5 ml of 2 mM or ronidazole (Lai et al., 2021) in PTU egg water or 1.5 ml of PTU egg water at 28.5°C in dark conditions for 6 h prior to imaging and for the duration of imaging.

2.8 | Whole mount immunohistochemistry

Following injury, 5–6 dpf larvae were fixed in AB Fix (4% PFA, 0.1% Triton X-100, 1X PBS) for either 3 h at 23°C or overnight at 4°C. Fixed larvae were then washed for 5 min with PBSTx (1% Triton X-100, 1X PBS) followed by a 5-minute wash with DWTx (1% Triton X-100, distilled water), a 5-minute wash with acetone at 23°C, a 10-minute wash with acetone at −20°C, and three 5-minute washes with PBSTx. Larvae were preblocked in 5% goat serum/PBSTx for a minimum of 1 h at 23°C and incubated in primary antibody for 1 h at 23°C and overnight at 4°C. The primary antibodies used in these studies include the following: a rabbit antibody to anti-phospho-Smad3 (1:175, Abcam catalog #ab52903) (Casari et al., 2014) and a chicken antibody to anti-GFP (1:200, Abcam catalog #ab13970). Larvae were washed with 1X PBSTx, preblocked in 5% goat serum/PBSTx for a minimum of 1 h at 23°C and incubated in secondary antibody for 1 h at 23°C and overnight at 4°C. Secondary antibodies used in these studies include the following: goat anti-rabbit IgG (H + L) cross-absorbed secondary antibody, Alex Fluor 647 (ThermoFisher Scientific catalog #A-21244) and goat anti-chicken IgY (H + L) cross-absorbed secondary antibody, Alexa Fluor 488 (ThermoFisher Scientific catalog # A-11039). Larvae were washed with 1X PBSTx and stored in 50% glycerol-PBS at 4°C until imaging. Larvae were mounted on their sides in 0.8% low-gelling point agarose on glass-bottom 35 mm Petri dishes and imaged using the confocal microscope and techniques described above. Image processing and alterations were limited to contrast enhancement and level settings were made using MetaMorph software and FIJI (ImageJ). 3D renderings were produced using Imaris (Oxford Instruments).

2.9 | Genotyping

DNA samples were prepared for individual *ctgfa*^{bns50} larvae after imaging by digesting larvae using HotSHOT (Meeker et al., 2007) and were amplified using the primers 5′-CATCTCCGTCCCACAGCCA-3′ and 5′-ACAGCACCGTCCAGACACG-3′ (Mokalled et al., 2016).

For pSmad3 antibody staining experiments conducted with *ctgfa*^{bns50} larvae, DNA was extracted from 3 dpf *ctgfa*^{bns50} larvae prior to injury and fixation using a Zebrafish Embryonic Genotyper (ZEG) (Danio Lab) and amplified using the same primers described above. Larvae selected for imaging were genotyped a second time following antibody staining using the method described above to confirm their genotype.

2.10 | Data collection

None of the data collected in these studies were blinded with the exception of the experiments conducted in *ctgfa*^{bns50} larvae in Figure 9. For these studies, 5 or 6 dpf larvae were injured using the nerve transection assay described above and time-lapse imaged every 2 h for 6 hpi. At 6 hpi, the larvae were unmounted and digested using HotSHOT (Meeker et al., 2007) for genotyping. Time-lapse movies were analyzed prior to completion of genotyping. *ctgfa*$^{-/-}$ larvae are morphologically indistinguishable from *ctgfa*$^{+/-}$ and *ctgfa*$^{+/+}$ larvae and therefore, require genotyping for identification.

2.11 | Quantification of perineurial glial and Schwann cell bridging

To quantify and compare the efficacy of bridging in either *nkx2.2a*:*megfp* or *sox10*:*megfp* larvae treated with either 10 μM SB431542 in 1% DMSO or 1% DMSO alone, we calculated the ratio of the size of

the bridge across the injury gap compared to the size of the original injury gap. Values greater than 1 indicate that perineurial glia (Figure 3g) or Schwann cells (Figure 3h) have fully bridged the original injury gap and continue to bridge past the initial distal stump. Values less than 1 indicate that perineurial glia or Schwann cells have not fully bridged the original injury gap, with negative values indicating the cells have retracted away from the injury site. The size of the initial injury gap was measured from a still image from each time-lapse movie at 0 hpi. The length of the injury gap bridged was measured from still images at each 30-minute time interval in each time-lapse movie over 8 h. The measured bridge size/measured size of the initial injury gap calculated for each time point and was repeated for each time-lapse movie captured for each group. These values were then plotted over time in 30-minute intervals for the duration of the 8-h time-lapse movie, with each dot representing the ratio of injury gap bridged: initial injury gap at a given time-point and with each line connecting the individual time-points from a single time-lapse movie. Each line represents an 8-h time-lapse movie of a single injury spinal motor nerve in a single 5 or 6 dpf larvae. Lines that end prior to the 8-h mark indicate time-lapse movies in which the injured larva died or the injured nerve shifted out of the imaging plane before the end of the time-lapse. All measurements were conducted using the manual measure tool in FIJI (ImageJ).

2.12 | Quantification of perineurial glial velocity

To quantify and compare the velocity of perineurial glial bridging in larvae treated with either 10 μM SB431542 in 1% DMSO or 1% DMSO alone, the position of the edge of either the proximal or distal perineurial glial stump from an individual time-lapse movie was tracked over each time point using the manual tracking plugin in FIJI (ImageJ). The positioning of the perineurial glial proximal and distal stumps was independently measured in 5-min intervals for the first 200 min post injury (mpi). The manual tracking plugin provides velocity measurements for each time point tracked. Each tracking was repeated three times and an average of the velocities was taken for each time point. This process was repeated for each time-lapse movie captured for each group (SB431542 or DMSO-treated larvae in proximal (proximal only), proximal (proximal and distal), and distal (proximal and distal) groups). The average velocity from each time-lapse movie in a group was then averaged at each time point and plotted over time, with each dot representing the average velocity at each time point in 5-min intervals and the lines connecting each group. To compare the average velocities between DMSO and SB431542-treated groups over the first 200 mpi, the average velocities for each group at each time point (every 5 min) over the 200 mpi time-lapse movie were plotted for both proximal and distal measurements. Each dot in the plot represents the average velocity of a single time-point over the 200 mpi time-lapse for all larvae in that group. An unpaired *t*-test was conducted for each plot to determine any significance between the average velocities of DMSO or SB431542-treated groups.

2.13 | Data quantification and statistical analyses

All graphically presented data represent the mean of the analyzed data. Statistical analyses and graphing were performed using GraphPad Prism software. *p* values involving only two groups were calculated using an unpaired student's *t* test. *p* values involving categorical groups were calculated using a Chi-square test. Significance levels were determined using a confidence interval of 95%. The data in the plots and in the text are presented as means ± SEM.

3 | RESULTS

3.1 | Perineurial glia bridge and phagocytose debris after spinal motor nerve injury

In zebrafish, peripheral motor nerve axons originate in the ventral ventricular, or pMN, domain of the spinal cord, migrating through the motor exit point transition zone into the periphery during early development (Myers et al., 1986; Park et al., 2002). Following the growing axons, Schwann cell precursors migrate from the dorsal neural tube into the periphery to differentiate into mature Schwann cells and myelinate axons within nerves (Lyons & Talbot, 2015). Perineurial glia then exit the spinal cord and begin to ensheath the Schwann cell-axon bundles at approximately 52 hpf (Kucenas, Takada, et al., 2008). By 5 days post-fertilization (dpf), zebrafish spinal motor nerves and their associated glia have matured past major developmental processes (Binari et al., 2013; Lewis & Kucenas, 2014; Rosenberg et al., 2012). This, along with the highly regenerative capacity of zebrafish (Ghosh & Hui, 2016; Marques et al., 2019; Mokalled & Poss, 2018; Poss et al., 2002; Shi et al., 2015), makes the larval zebrafish an optimal model for studying motor nerve regeneration.

Using *nkx2.2a:megfp* to label perineurial glia and *olig2:dsred* to label motor axons (Kucenas, Snell, & Appel, 2008; Lewis & Kucenas, 2014) (Figure 1a), we injured peripheral spinal motor nerves in 5 or 6 dpf zebrafish larvae on either the caudal or rostral tract of the nerve using laser axotomy as previously described (Lewis & Kucenas, 2013; A. F. Rosenberg et al., 2012; Allison F. Rosenberg et al., 2014) and time-lapse imaged every 5 min for 8 h post injury (hpi). Consistent with previous studies (Lewis & Kucenas, 2014), we observed perineurial glia with phagocytic vesicles primarily proximal to the injury site between 1 and 6 hpi, a behavior we previously observed via labeling with LysoTracker (Figure 1b; $n = 11$ nerves in 5 larvae) (Lewis & Kucenas, 2014). Additionally, we observed perineurial glia form a complete bridge across the injury gap within the first 6 hpi in both rostral and caudal nerve tract injuries (Figure 1b; $n = 11$ nerves in 5 larvae). Perineurial glial bridging and phagocytosis is crucial for motor nerve regeneration (Lewis & Kucenas, 2014). However not much is known about the dynamics of these processes nor the identity of the signals that drive these cellular behaviors.

To begin to characterize perineurial glial bridging, we analyzed the time at which perineurial glia initiated and completed bridging. We defined bridging initiation as perineurial glial membranes crossing

beyond the proximal or distal injury stump and bridging completion as perineurial glial membranes fully bridging across the original injury gap. For these analyses, we used time-lapse videos of motor nerves injured on either the rostral or the caudal tract in 5 or 6 dpf *nkx2.2a:megfp;olig2:dsred* larvae. Our results showed that the majority of perineurial glia initiate bridging within the first 2 hpi ($n = 9$ nerves in 5 larvae), with all perineurial glia initiating bridging within the first 6 hpi (Figure 1c; $n = 11$ nerves in 5 larvae). Additionally, the majority of perineurial glia complete bridging by 5 hpi ($n = 9$ nerves in 5 larvae), with all bridging complete by 8 hpi ($n = 11$ nerves in 5 larvae) and with an average total bridging time of approximately 2.5 h (Figure 1d; mean: 150.54 min). In our studies, we also observed that when perineurial glia bridge, they either bridge from both the proximal and distal sides of the injury, with perineurial glia meeting in the middle ($n = 6$ nerves in 5 larvae), or from only the proximal side of the injury, with perineurial glia extending from the proximal stump fully across the injury site ($n = 5$ nerves in 5 larvae). Each type of bridging is equally likely to occur, and there is no difference in bridging timing between the two different types (Figure 1c,e).

In addition to bridging the injury gap, perineurial glia form phagocytic vesicles to clear axonal debris shortly after injury (Lewis & Kucenas, 2014). To further characterize perineurial glial phagocytosis, we investigated whether there was a difference in where phagocytic vesicles formed in perineurial glia using the same time-lapse videos of perineurial glial bridging used in the previous analyses (Figure 1b–d). Although half of the injured nerves had bridging from perineurial glia on both the proximal and distal side of the injury site, we observed that the majority (73%) of perineurial phagocytic vesicles were formed only on the proximal side of the nerve (Figure 1f; $n = 8$ nerves in 5 larvae). While some injured nerves did have vesicles on both the proximal and distal side of the injury (Figure 1f; $n = 3$ nerves in 5 larvae), no injured nerves had phagocytic vesicles in only perineurial glia distal to the injury (Figure 1f). These analyses confirm that perineurial glia play a pivotal role early in the regeneration process by forming a bridge across the injury gap and phagocytosing debris.

Together, this data establishes a timeline during which perineurial glial bridging occurs (Figure 1g). During the first 4 hpi, perineurial glia initiate bridging and phagocytose debris, providing by 6–8 hpi, a scaffold upon which the injured nerve can regenerate. During this time, macrophages infiltrate the injury site to clear debris and Schwann cells begin to activate their repair program, which occurs during the first 12 hpf (Chen et al., 2015; Jessen et al., 2015; Jessen & Mirsky, 2016; Lewis & Kucenas, 2014). Between 12 to 24 hpi, following perineurial glial bridge completion, Schwann cells form Bands of Bungner to guide regenerating axons across the injury site to re-innervate target tissues (Jessen & Mirsky, 2016; Min et al., 2021). Importantly, Schwann cells do not form Bands of Bungner across the injury site until after perineurial glial bridging is complete and full spinal motor nerve regeneration takes between 24 and 48 hpi in zebrafish larvae (Lewis & Kucenas, 2014; Rosenberg et al., 2012; Rosenberg et al., 2014). For our studies in this manuscript, we focused on the first 8 during which perineurial glia are bridging and phagocytosing debris (Figure 1g). While these perineurial glial behaviors are critical for efficient regeneration, not much is known about bridging dynamics or the molecular signals that regulate these events.

3.2 | Perineurial glia do not proliferate after spinal motor nerve injury

To further elucidate perineurial glial bridging dynamics, we explored the role that the positioning of perineurial glial cells along the nerve plays in bridging. We first examined the number of *nkx2.2a*$^+$ nuclei present on the nerve. Using *nkx2.2a:nls-egfp* or *nkx2.2a:nls-mch* to visualize perineurial glia nuclei (Fontenas & Kucenas, 2021; Kucenas, Snell, & Appel, 2008; Zhu et al., 2019), we imaged *nkx2.2a*$^+$ nuclei at both 5 and 6 dpf. The number of *nkx2.2a*$^+$ nuclei as well as the position of the nuclei along the nerve varied per nerve, but there was no significant change in the number of cells between 5 and 6 dpf (Figure 2a; 5 dpf: $n = 10$ nerves in 5 larvae, mean: 4.8 nuclei; 6 dpf: $n = 17$ nerves in 5 larvae, mean: 6.1 nuclei). Next, we asked whether perineurial glia proliferated in order to form the bridge after injury. Using *nkx2.2a:nls-mcherry*; *olig2:dsred* larvae to label perineurial glial nuclei and motor axons, respectively, we performed laser axotomy and time-lapse imaged for 6 hpi. In these studies, we observed Wallerian degeneration, however *nkx2.2a*$^+$ nuclei did not migrate or divide (Figure 2b; $n = 4$ nerves in 3 larvae). This indicates that when perineurial glia form a bridge, the cell bodies do not migrate and perineurial glia do not proliferate. Instead, perineurial glia extend membrane processes across the injury site.

Finally, we analyzed the role that perineurial glial nuclei position plays in the types of perineurial glial bridging that we observed. We hypothesized that positioning of perineurial glia nuclei relative to the injury site would affect the type of bridging that occurs. Following injury to larvae expressing *nkx2.2a:megfp* and *nkx2.2a:nls-mcherry* to label perineurial glial membranes and nuclei, respectively, we observed two distinct types of bridging on both the rostral and caudal side of the nerve, consistent with our previous imaging (Figure 1e). We observed that when an injury is created with no *nkx2.2a*$^+$ nuclei distal to the injury site, perineurial glia proximal to the injury site extend their membrane fully across the injury gap (Figure 2c; $n = 6$ nerves in 4 larvae). This likely occurs because when no *nkx2.2a*$^+$ nuclei are distal to the injury site, the remaining perineurial glial membrane distal to the injury degenerates away with the nerve. Conversely, perineurial glial membranes both proximal and distal to the injury site actively bridged when *nkx2.2a*$^+$ nuclei were present on both sides of the injury site (Figure 2c; $n = 4$ nerves in 3 larvae). Both types of bridging occurred on a similar time scale, with bridging initiating by 2 hpi and completing by 6 hpi (data not shown). Therefore, the difference in bridging we observed was due to location of the injury site relative to the position of *nkx2.2a*$^+$ nuclei. Similar to the *nkx2.2a*$^+$ nuclei imaged with *olig2:dsred* (Figure 2b), *nkx2.2a*$^+$ nuclei did not migrate or divide along nerves that exhibited either type of bridging (Figure 2c, $n = 10$ nerves in 7 larvae). Overall, these studies demonstrate that perineurial glial

bridging behaviors are not due to cell migration or division. Instead, the positioning of *nkx2.2a*$^{+}$ nuclei relative to the injury influences how perineurial glia bridge.

3.3 | Inhibition of TGFβ signaling perturbs perineurial glial bridging but not phagocytosis

We know that perineurial glia form a bridge within the first 1–4 hpi and complete their membrane extension across the bridge by 6–8 hpi, phagocytosing axonal debris as they bridge (Figure 1c,d) (Lewis & Kucenas, 2014). However, it remains unknown what molecular signals drive this process. Transforming growth factor-beta (TGFβ) signaling is an established regulator of regenerative processes (Keatinge et al., 2021; Kim et al., 2006; Lenkowski et al., 2013; Nakamura et al., 2021; Sharma et al., 2020; Sulaiman & Nguyen, 2016), specifically during motor nerve regeneration (Clements et al., 2017; Frostick et al., 1998; Schira et al., 2018). TGFβ-1 is important for the Schwann cell repair program, and Schwann cells both secrete TGFβ-1 following injury (Schira et al., 2018) and require it to successfully migrate across the injury site (Clements et al., 2017). Additionally, TGFβ-1 is secreted by macrophages responding to injury, providing a source of TGFβ-1 for Schwann cells (Chen et al., 2021). Finally, TGFβ signaling is also important for perineurial glial development (Morris et al., 2017). Therefore, because TGFβ signaling is present during motor nerve regeneration and perineurial glia require TGFβ for development, we hypothesized that TGFβ signaling might also drive perineurial glial bridging after injury.

To investigate the role of TGFβ signaling in perineurial glial bridging, we treated 4 dpf *nkx2.2a:megfp;olig2:dsred* larvae with either 10 μM SB431542, a selective inhibitor of the TGFβ-1 receptor, dissolved in 1% DMSO, or 1% DMSO alone for 48 h (Morris et al., 2017; Sun et al., 2006) prior to injury. In these studies, larvae were treated from 4 to 6 dpf, a window after which perineurial glia have fully ensheathed the nerve and undergone their major developmental processes (Kucenas, 2015; Kucenas, Snell, & Appel, 2008; Kucenas, Takada, et al., 2008; Lewis & Kucenas, 2014). Larvae in both SB4315342 and DMSO-treated groups showed no changes in overall morphology, motor nerve development, or perineurial glial ensheathment of the nerve after treatment (Figure S1; $n = 11$ nerves in 5 fish, 14 nerves in 6 fish, respectively) (Morris et al., 2017; Sun et al., 2006). We then used laser axotomy to injure spinal motor nerves in both SB431542 and DMSO-treated groups. After time-lapse imaging for 8 hpi, we observed that perineurial glia in 1% DMSO-treated control larvae formed phagocytic vesicles and initiated bridging within 2 hpi, with bridging complete by 4 to 6 hpi, consistent with our previous data (Figure 3a-a"; $n = 5$ nerves in 4 larvae) (Movie S1). In contrast, perineurial glia in larvae treated with 10 μM SB431542 formed phagocytic vesicles but did not initiate bridging or cross over the injury site by 8 hpi (Figure 3d-d", $n = 6$ nerves in 4 larvae) (Movie S2). We observed bridging in all DMSO controls ($n = 5$ nerves in 4 larvae) but in none of the TGFβ inhibitor-treated larvae ($n = 6$ nerves in 4 larvae) (Figure 3g). Additionally, in some cases, perineurial glia in SB431542-treated larvae that failed to bridge began to degenerate along with the nerve, resulting in a larger gap between the perineurial glial stump and the original injury site (Figure 3g). From these studies we conclude that inhibition of TGFβ signaling perturbs perineurial glial bridging after injury.

To determine if these changes in perineurial glial bridging behaviors were specific to perineurial glia and not due to a change in behavior of other cells involved in the injury response (Figure 1g), we repeated these experiments using either *sox10:megfp* to label Schwann cells or *mpeg1:egfp* to label macrophages with *olig2:dsred* to label motor axons. Both groups of transgenic larvae were treated with either 10 μM SB431542 in 1% DMSO or 1% DMSO alone for 48 h from 4 to 6 dpf prior to injury and time-lapse imaged for 8 hpi. Previous studies demonstrate that immediately following injury, Schwann cells extend processes towards the injury site, but do not migrate into it within the first 8 hpi (Lewis & Kucenas, 2014). Consistent with this, we observed no difference in the migration of Schwann cells in *sox10:megfp* larvae treated with DMSO ($n = 4$ nerves in 3 larvae) or SB431542 ($n = 4$ nerves in 3 larvae) (Figure 3b-b",e–e",h). Similarly, *mpeg1:egfp* larvae treated with DMSO ($n = 8$ nerves in 5 larvae) or SB431542 ($n = 6$ nerves in 4 larvae) showed no difference in the number of macrophages recruited to the injury site nor the timing of macrophages entering the injury site (Figure 3c-c",f-f",i,j). These results demonstrate that inhibition of TGFβ signaling disrupts perineurial glial bridging but not phagocytosis, without perturbing the early injury responses of either Schwann cells or macrophages during the first 8 hpi. Therefore, perineurial glial bridging and phagocytosis are two behaviors controlled by separate molecular signals and inhibition of TGFβ signaling perturbs perineurial glial bridging independent of Schwann cell and macrophage behaviors.

To further confirm that the vesicles observed in SB431542-treated perineurial glia were indicative of phagocytosis of axonal debris, we utilized Imaris (Oxford Instruments) to render 3D images of 5 or 6 dpf *nkx2.2a:megfp;olig2:dsred* larvae treated with either 1% DMSO ($n = 5$ nerves in 4 larvae) or 10 μM SB431542 in 1% DMSO ($n = 6$ nerves in 4 larvae). 3D rendering demonstrated that axonal debris observed in perineurial glial vesicles in our time-lapse imaging in the first 3 hpi were fully engulfed by perineurial glial membranes in both DMSO-treated (Figure 4a) and SB431542-treated (Figure 4b) larvae. Therefore, although SB431542-treated perineurial glia were unable to form a glial bridge across they injury site, we continued to observe them phagocytosing debris (Figure 4c).

3.4 | TGFβ signaling is present during early phases of perineurial glial bridging

We next wanted to explore the timing during which TGFβ signaling is impacting perineurial glial bridging. Because inhibition of TGFβ signaling prevented perineurial glia from crossing into the injury site, we hypothesized that TGFβ signaling is important for early initiation of this behavior. To explore this, we injured 5 or 6 dpf *nkx2.2a:nls-egfp;olig2:dsred* larvae and fixed the larvae at 2, 3, or 6 hpi. For these

studies, we used uninjured sibling larvae as controls. We then stained all groups with an antibody specific to phosphorylated Smad3 (pSmad3), an indicator of active TGFβ signaling (Casari et al., 2014; Kitisin et al., 2007; Morris et al., 2017). In these studies, using Imaris (Oxford Instruments) to render 3D images of *nkx2.2a*$^+$ nuclei and pSmad3 labeling, we did not observe any pSmad3-positive *nkx2.2a*$^+$ nuclei along uninjured spinal motor nerves (Figure 5a; $n = 13$ nerves in 9 larvae). However, we did see pSmad3 labeling in *nkx2.2a*$^+$ nuclei at 2, 3, and 6 hpi (Figure 5b–d; 2 hpi, $n = 20$ nerves in 4 larvae; 3 hpi, $n = 21$ nerves in 6 larvae; 6 hpi, $n = 17$ nerves in 4 larvae). The percentage of nerves with pSmad3$^+$/*nkx2.2a*$^+$ nuclei increased at 3 hpi and decreased by 6 hpi (Figure 5f). From these data we observed the most pSmad3$^+$ perineurial glial nuclei at 3 hpi, the time at which perineurial glia are actively bridging. Importantly, we did not observe pSmad3 staining in *nkx2.2a*$^+$ nuclei at 3 hpi in larvae treated with 10 μM SB431542 (Figure 5e; $n = 15$ nerves in 5 larvae). This is consistent with our data demonstrating that perineurial glia do not initiate bridging into the injury gap with inhibition of TGFβ signaling (Figure 3d).

In addition to pSmad3 staining in *nkx2.2a*$^+$ nuclei, we also observed pSmad3 staining along the injured nerve in linear structures, but not along uninjured nerves or nerves treated with 10 μM SB431542 (Figure 5a–e; uninjured, $n = 13$ nerves in 9 larvae; 2 hpi $n = 20$ nerves in 4 larvae; 3 hpi, $n = 21$ nerves in 6 larvae; 6 hpi, $n = 17$ nerves in 4 larvae; SB431542 treatment, $n = 15$ nerves in 5 larvae). The percentage of nerves with pSmad3 staining along the injured nerve increased over time following injury, with pSmad3 staining largely present along both the proximal and distal stump (Figure 5g; 2 hpi, $n = 20$ nerves in 4 larvae; 3 hpi, $n = 21$ nerves in 6 larvae; 6 hpi, $n = 17$ nerves in 4 larvae). Because the percentage of nerves with pSmad3 staining along the injured nerve is highest at 6 hpi, when perineurial glia complete bridging, it is possible that this pSmad3 labeling we observed was present in bridged perineurial glial, as the distal axon has mostly degenerated by that time but has not yet begun to regenerate. Therefore, we conclude that TGFβ signaling is important for early initiation of perineurial glial bridging.

3.5 | Inhibition of TGFβ signaling alters perineurial glial bridging dynamics

Taken together, our data demonstrates that TGFβ signaling is essential for perineurial glial bridging. To further elucidate how TGFβ signaling is affecting perineurial glial bridging, we decided to explore the effect of TGFβ inhibition on bridging dynamics. To do this, we measured the velocity of perineurial glial membrane processes after injury. Velocity was measured by manually tracking perineurial glia on both proximal and distal stumps (Figure 6a) over a period of 8 hpi from time-lapse movies taken from injured 6 dpf *nkx2.2a:megfp;olig2:dsred* larvae treated with either 1% DMSO or 10 μM SB431542 in 1% DMSO. Our tracking demonstrated that in larvae treated with SB431542, perineurial glia did not bridge the injury gap (Figure 6c). In contrast, we observed both perineurial glial stumps meeting in the middle of the injury gap in DMSO-treated larvae (Figure 6b). We then plotted average velocity in μm/second against time in minutes post injury for the first 200 min post injury, the period during which perineurial glial bridging initiates. Velocities were measured for the proximal stump in nerves that only had proximal bridging, for the proximal stump in nerves that had both proximal and distal bridging, and for the distal stump in nerves that had both proximal and distal bridging in both DMSO and SB431542-treated larvae. Intriguingly, there was no difference in bridging velocity between SB431542-treated and DMSO-treated larvae for nerves where only the proximal side bridged (Figure 6d,g; DMSO-treated, $n = 3$ nerves in 3 larvae; *SB431542-treated*, $n = 3$ nerves in 3 larvae). However, there was a significantly higher velocity in both proximal bridging velocity and distal bridging velocity in DMSO-treated larvae compared to SB431542-treated larvae for nerves that had both proximal and distal bridging (Figure 6e,f,h,i; *DMSO-treated*, $n = 4$ nerves in 3 larvae, *SB431542*-treated, $n = 3$ nerves in 3 larvae). These differences in perineurial glial bridging velocity in DMSO-treated larvae compared to SB431542-treated larvae further demonstrate that TGFβ signaling is essential for initiation of perineurial glial bridging across the injury gap. However, the source of this TGFβ signaling remains unknown.

3.6 | Absence of Schwann cells immediately prior to injury perturbs perineurial glial bridging

Schwann cells are known to both secrete TGFβ-1 following nerve injury (Schira et al., 2018; Sulaiman & Nguyen, 2016) and require TGFβ signaling to drive their own directional migration across the injury site (Clements et al., 2017). Therefore, Schwann cells are a potential source of TGFβ-1 during perineurial glial bridging. Previous studies from our lab demonstrate that in the absence of Schwann cells, perineurial glia fail to form a glial bridge after spinal motor nerve injury (Lewis & Kucenas, 2014). However, these studies were conducted in colorless mutants, which are deficient in *sox10* and lack Schwann cells during development (Dutton et al., 2001). Because perineurial glia require Schwann cells for proper development (Morris et al., 2017), perineurial glia in colorless mutants were sparse and did not fully ensheath nerves (Lewis & Kucenas, 2014). Therefore, nerve regeneration was likely not completely wildtype.

To determine if Schwann cells are required for perineurial glial bridging and a possible source of TGFβ-1, we injured motor nerves in 5 or 6 dpf *nkx2.2a:megfp;sox10:gal4;UAS:NTR-mcherry* larvae. Prior to injury, larvae were either kept in PTU egg water or treated with 2 mM ronidazole (RDZ) in PTU egg water for 6 h to induce the expression of nitroreductase and subsequent cell-specific death in *sox10*$^+$ cells (Lai et al., 2021). In these studies, we observed that *sox10*$^+$ Schwann cells in RDZ-treated larvae were successfully ablated when imaging began. However, perineurial glial ensheathment of spinal motor nerves appeared healthy and intact (data not shown). Following spinal motor nerve injury, larvae in PTU egg water displayed perineurial glial bridging and phagocytosis by 6 hpi (Figure 7a,c; $n = 4$ nerves in 3 larvae). However, perineurial glia in larvae treated with RDZ did not bridge by

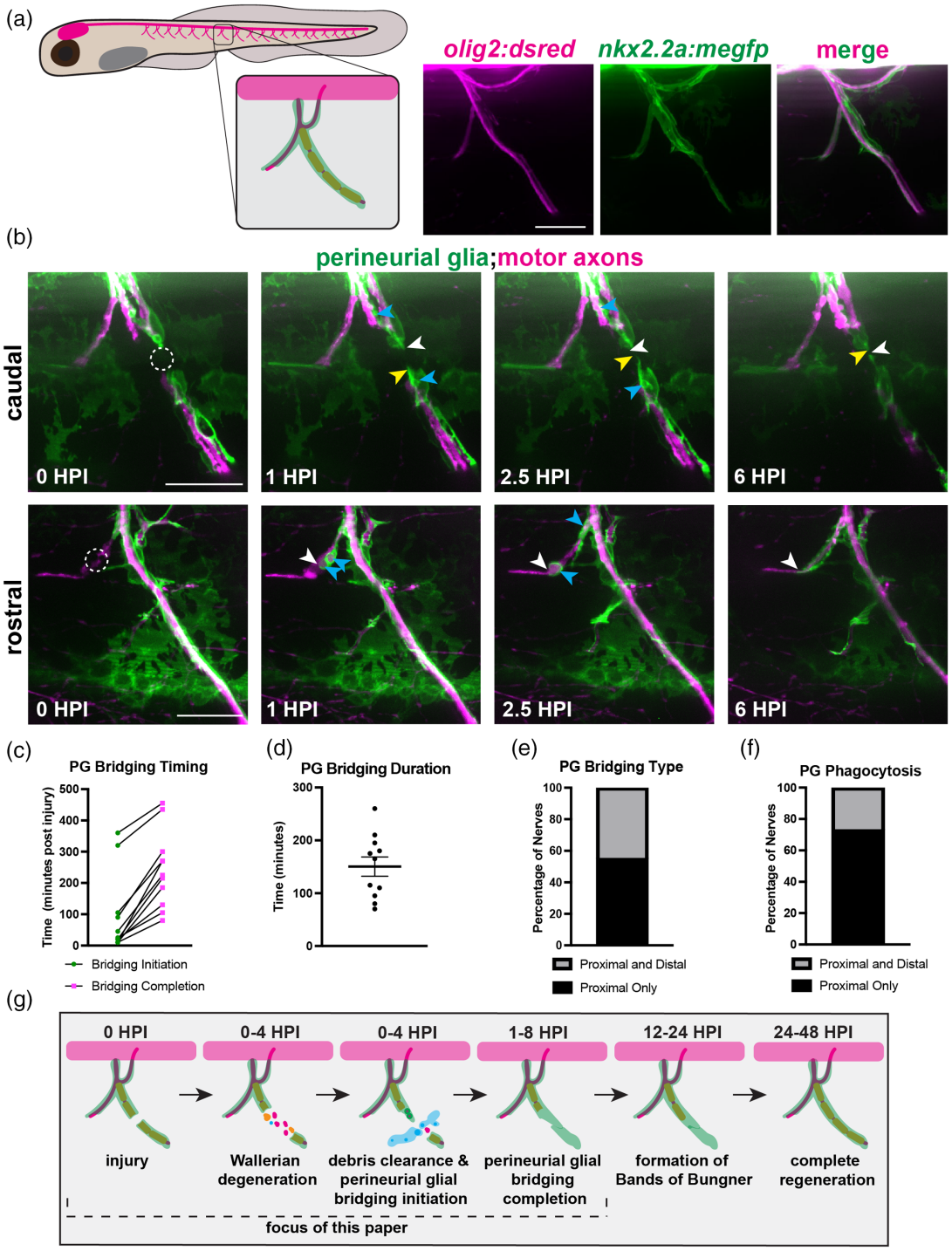

FIGURE 1 Perineurial glia form a bridge and phagocytose debris after spinal motor nerve injury. (a) (Left) Diagrammatic representation of a 6 dpf zebrafish larva with a single peripheral spinal motor nerve (inset) displayed. Motor axon (magenta), ensheathed Schwann cells (orange), perineurial glia (green). (Right) Representative images of an in vivo 6 dpf spinal motor nerve, where *olig2* labels motor axons (magenta) and *nkx2.2a* labels perineurial glia (green). (b–f) $n = 11$ nerves in 5 larvae. (b) Representative stills taken from time-lapse movies of perineurial glia (green) and motor axons (magenta) in 5 or 6 dpf larvae injured on either the caudal or rostral side of the spinal motor nerve. Stills are shown in the first 6 h post injury (hpi). The dashed circle indicates the injury site. Blue arrows denote phagocytic vesicles in perineurial glia. White arrows follow the proximal end and yellow arrows follow the distal end of the perineurial glial bridge. (c) Quantification of perineurial glial (PG) bridging timing. Timing of bridging initiation (green) and completion (magenta) was recorded in minutes post injury. (d) Quantification of perineurial glial (PG) bridging duration in minutes (mean: 150.54 ± 18.25 min). (e) Quantification of the type of perineurial glial (PG) bridging observed. Proximal and distal bridging (45% of nerves, gray) or proximal only bridging (55% of nerves, black). (f) Quantification of perineurial glial (PG) phagocytosis after injury. Phagocytic vesicles on both proximal and distal perineurial glial stumps (27% of nerves, gray) or only on proximal perineurial glial stumps (73% of nerves, black). (g) Representative timeline of the first 48 h following spinal motor nerve injury in 5 to 6 dpf zebrafish. Motor axon (magenta), Schwann cells (orange), perineurial glia (green), macrophages (blue). Scale bars, 25 μm.

6 hpi (Figure 7b,c; $n = 7$ nerves in 5 larvae). Therefore, in the absence of Schwann cells, perineurial glia were unable to bridge, indicating that perineurial glia might require signals from Schwann cells to successfully bridge the injury site. Interestingly, we did observe that perineurial glia continue to phagocytose debris in RDZ-treated larvae, reinforcing the hypothesis that perineurial glial bridging and phagocytosis are distinct events controlled by different molecular cues (Figures 3d and 7b). However, perineurial glia do not appear to phagocytose Schwann cell debris in RDZ-treated larvae. This indicates that perineurial glial phagocytosis is specific to axonal debris and that the signals that drive phagocytosis are not derived from Schwann cells. This observation is consistent with previous data suggesting that Schwann cells, macrophages, and perineurial glia spatially coordinate their debris clearance following injury (Lewis & Kucenas, 2014). Taken together, our data are consistent with the hypothesis that there is communication occurring between Schwann cells and perineurial glia following injury that drives perineurial glial bridging, indicating Schwann cells as a possible source of perineurial glial-dependent TGFβ signaling, though future studies will need to be conducted to confirm this hypothesis.

3.7 | Connective tissue growth factor-a is expressed in the periphery following injury

Because inhibition of TGFβ signaling perturbs perineurial glial bridging initiation, we next wanted to identify other components of TGFβ signaling that may also be involved in this process. We decided to explore the expression of connective tissue growth factor a (*ctgfa*), a gene that is actively involved in wound healing (Mokalled et al., 2016; Mukherjee et al., 2021; Zhang et al., 2021). *ctgfa* is expressed downstream of TGFβ signaling and works in a positive feedback loop to enhance receptor binding of TGFβ-1 (Abreu et al., 2002; Mukherjee et al., 2021; Zaykov & Chaqour, 2021; Zhang et al., 2021). Following peripheral nerve injury, CTGF is secreted by Schwann cells, which provides a potential source for both TGFβ and *ctgfa* signaling (Schira et al., 2018). Additionally, *ctgfa* is necessary and sufficient for glial bridging following spinal cord injury in zebrafish (Mokalled et al., 2016).

To determine if *ctgfa* is involved in perineurial glial bridging, we injured 6 dpf *ctgfa:egfp;olig2:dsred* larvae and imaged for 6 hpi to determine if *ctgfa* was expressed following injury. We used laser-induced transection to perform either no injury, injury to the muscle, or spinal motor nerve axotomy (Figure 8a–c). In larvae with either no injury or injury to the muscle, we saw no change in *ctgfa* expression over 6 hpi (Figure 8a-a",b-b"“; no injury, $n = 4$ nerves in 4 larvae; muscle injury, $n = 4$ nerves in 4 larvae). However, in larvae where we induced spinal motor nerve injury, we observed an increase in *ctgfa* expression in the injury site over 6 hpi (Figure 8c-c"; $n = 11$ nerves in 5 larvae). This data demonstrates that *ctgfa* expression is increased only after spinal motor nerve axotomy. Interestingly, we observed *ctgfa* expression within the injury site during the 2–6 hpi window that perineurial glia are bridging. Therefore, we hypothesized that *ctgfa* might drive perineurial glial bridging downstream of TGFβ signaling.

To assess the role of *ctgfa* expression in perineurial glial bridging, we created a *nkx2.2a:gal4;UAS:NTR-mcherry* line to visualize both perineurial glia and *ctgfa* expression after injury. We injured motor nerves in 5 or 6 dpf *nkx2.2a:gal4;UAS:NTR-mcherry;ctgfa:egfp* larvae using laser axotomy and time-lapse imaged for 8 hpi. Although we observed both perineurial glial bridging and an increase in *ctgfa* expression along all injured nerves, we did not observe co-localization of *nkx2.2a* and *ctgfa* expression (Figure 8d′-d″; $n = 6$ nerves in 4 larvae). Although *ctgfa* expression was not observed in perineurial glial cells after injury, it is possible that *ctgfa* drives perineurial glial bridging indirectly through its positive feedback loop with TGFβ signaling.

To determine whether *ctgfa* expression in the injury site was indeed downstream of TGFβ signaling, we treated 4 dpf *ctgfa;egfp; olig2:dsred* larvae with 10 μM SB431542 in 1% DMSO or 1% DMSO alone. Spinal nerves in larvae from both groups were injured and imaged for 6 hpi at 6 dpf. DMSO-treated larvae showed an increase in *ctgfa* expression in the injury site by 2 hpi, with expression in the injury site increasing through 6 hpi (Figure 8e-e" $n = 4$ nerves in 3 larvae). Larvae treated with SB431542 showed no change in expression of *ctgfa* after injury and had no increase in *ctgfa* in the injury site by 6 hpi (Figure 8f-f"; $n = 4$ nerves in 3 larvae). Therefore, inhibition of TGFβ signaling negatively regulates *ctgfa* expression in the injury site. Because *ctgfa* expression is changed by TGFβ signaling inhibition but is present in the injury site during the timing of perineurial glial bridging in the presence of TGFβ signaling, we hypothesized that *ctgfa* works within the TGFβ signaling pathway to drive perineurial glial bridging.

3.8 | Perineurial glial bridging, but not phagocytosis, is perturbed in ctgfa mutant larvae

To determine if *ctgfa* was required for perineurial glial bridging even in the presence of TGFβ signaling, we injured spinal motor axons in *ctgfa*^{bns50} larvae, which have a 7-nt deletion in the third exon of *ctgfa* (Mokalled et al., 2016). *ctgfa*$^{-/-}$ adults are viable and larvae at 6 dpf show typical motor nerve and perineurial glial development (Figure 9a). Larvae from an in-cross of *ctgfa*$^{+/-}$ fish expressing both *nkx2.2a:megfp* and *olig2:dsred* were injured at 5 or 6 dpf and time-lapse imaged in 2-h intervals for 6 hpi. Larvae were then genotyped immediately following the completion of imaging. In *ctgfa*$^{+/+}$ larvae, we always observed perineurial glial bridging within the first 6 hpi (Figure 9b,e,f; $n = 5$ nerves in 4 larvae). In contrast, perineurial glia fully bridged the injury site in only 55% of nerve axotomies in *ctgfa*$^{+/-}$ larvae (Figure 9c,e,f; $n = 10$ bridging nerves, $n = 9$ non-bridging nerves in 10 larvae). Finally, we observed no perineurial glial bridging along injured motor nerves in any *ctgfa*$^{-/-}$ larvae (Figure 9d,e,f; $n = 11$ nerves in 6 larvae). This phenotype is consistent with what we observed in SB431542-treated larvae (Figure 3d). Interestingly, perineurial glia continue to form phagocytic vesicles in all genotypes (Figure 9b–d,g). Therefore, because loss of *ctgfa* produces a similar phenotype to that of TGFβ inhibition, we conclude that *ctgfa* is required for perineurial glial bridging.

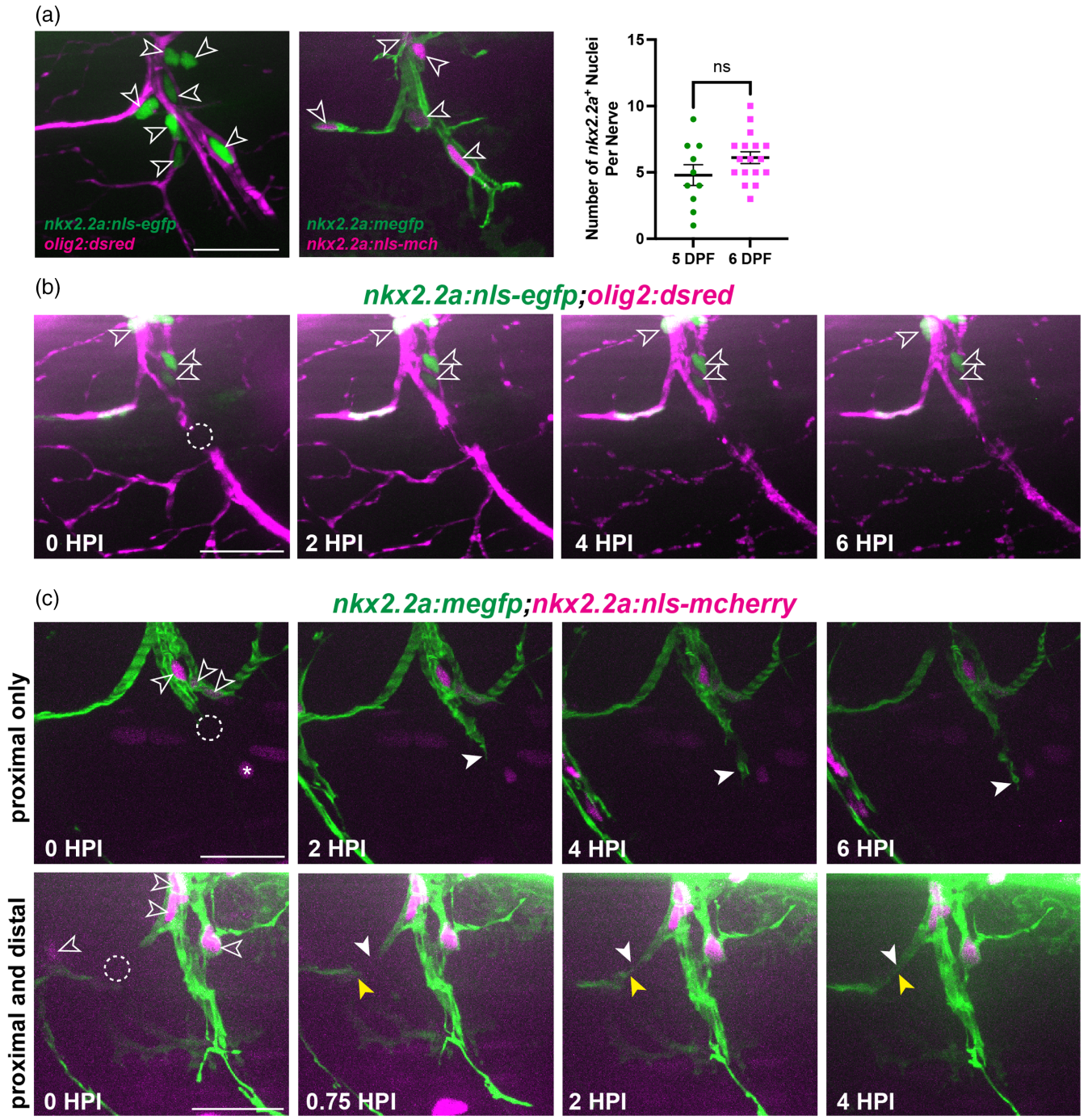

FIGURE 2 Perineurial glia do not proliferate following spinal motor nerve injury. (a) (Left) Representative images of perineurial glial nuclei (open arrows) imaged with either motor axons (magenta, left) or perineurial glial membrane (green, right) at 5 dpf. (Right) Quantification of the number of *nkx2.2a*$^{+}$ nuclei on a single spinal motor nerve in 5 (green, $n = 10$ nerves in 5 larvae, mean: 4.8 ± 0.79 nuclei) and 6 dpf (magenta, $n = 17$ nerves in 5 larvae, mean: 6.1 ± 0.44 nuclei) larvae ($p = .1272$). (b) Representative images from a time-lapse movie of *nkx2.2a*$^{+}$ nuclei (green) in an injured 6 dpf larva. The dashed circle indicates the injury site ($n = 4$ nerves in 3 larvae). (c) Representative still images from a time-lapse movie of *nkx2.2a*$^{+}$ nuclei (magenta, open arrowheads) in injured 5 to 6 dpf larvae exhibiting either proximal only bridging (top panels, $n = 6$ nerves in 4 larvae) or proximal and distal bridging (bottom panels, $n = 4$ nerves in 3 larvae). Solid white arrows follow the proximal end and yellow arrows follow the distal end of the perineurial glial bridge (green). Asterisks indicate *nkx2.2a*$^{+}$ cells that are not perineurial glial nuclei. Scale bars, 25 μm.

While our data demonstrates that both TGFβ signaling (Figure 3) and *ctgfa* (Figure 9) are required for perineurial glial bridging, we next wanted to determine if *ctgfa* and TGFβ signaling are working in a positive feedback loop to drive perineurial glial bridging. To explore this, we injured 5 or 6 dpf *nkx2.2a:nls-egfp;olig2:dsred ctgfa*$^{+/+}$, *ctgfa*$^{+/-}$, *or ctgfa*$^{-/-}$ larvae and fixed the larvae at 3 hpi. We then

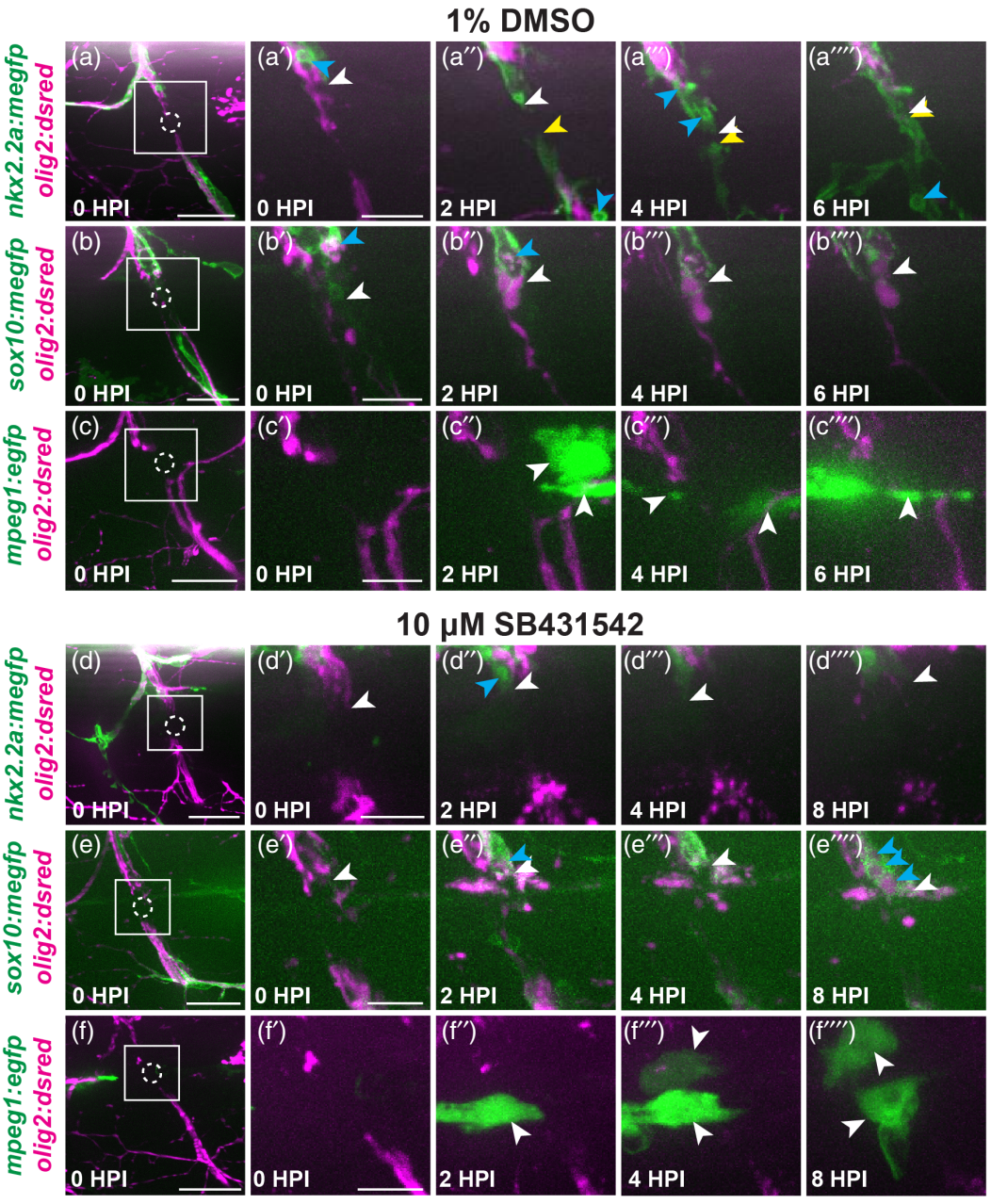

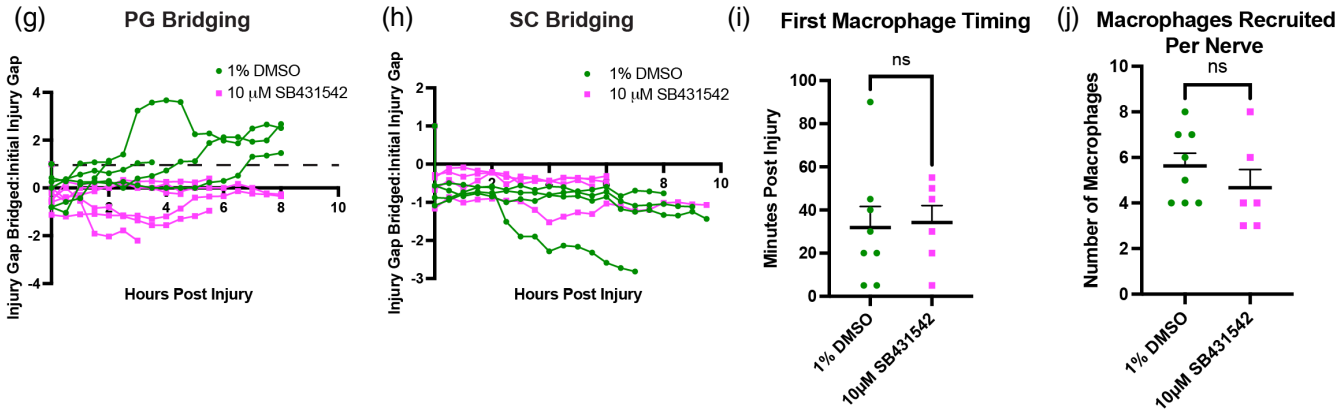

FIGURE 3 Legend on next page.

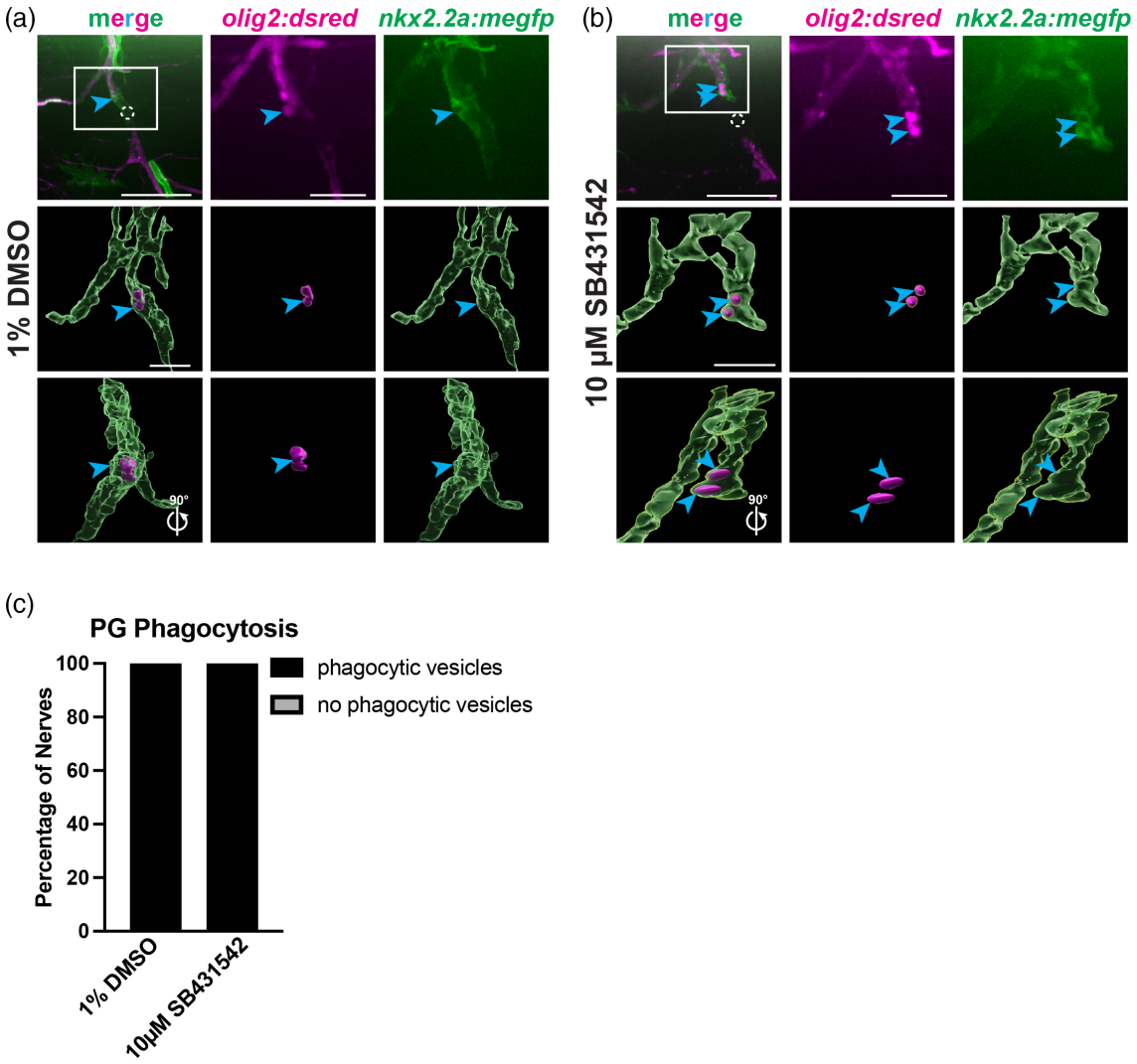

FIGURE 4 Phagocytosis is observed in perineurial glia with inhibition of TGFβ. (a,b) Representative images of 5 dpf *nkx2.2a:megfp;olig2:dsred* injured larvae treated with either 1% DMSO (a) or 10 μM SB431542 (b) at 3 hpi. The dashed circle indicates the injury site. Axonal debris and perineurial glial vesicles are specified by blue arrows. 3D renderings of these representative images are shown in both a 0° and 90° rotated views (Imaris). (c) Quantification of the presence of phagocytic vesicles in 1% DMSO or 10 μM SB431542 in 1% DMSO-treated larvae. Phagocytic vesicles were present in 100% of injured nerves in both groups ($n = 5$ nerves in 4 larvae, 6 nerves in 4 larvae, respectively). Scale bars, 25 μm; magnified insets and 3D renderings, 10 μm.

FIGURE 3 Inhibition of TGFβ signaling perturbs perineurial glial bridging. (a–f) Representative stills from time-lapse movies of 5–6 dpf larvae with injured spinal motor nerves (magenta) treated with either 1% DMSO (a–c) or 10 μM SB431542 (d–f). The dashed circle indicates the injury site while the solid line box indicates the regions of interest highlighted in adjacent insets. Blue arrows specify phagocytic vesicles. (a,d) White arrows follow the proximal end and yellow arrows follow the distal end of the perineurial glial bridge (green). (b,e) White arrows follow the proximal Schwann cell stump (green). (c,f) White arrows show macrophages (green) present in the injury site. (g,h) Quantification of either perineurial glial (PG) bridging (g) or Schwann cell (SC) bridging (h) over 8 hpi in both DMSO (green) and SB431542-treated (magenta) groups. Measurements of perineurial glial membrane (g) or Schwann cell (h) extension into the injury site were compared to the size of the initial injury gap, with values over 1 (dotted-line) indicating complete bridging and values less than zero indicating retraction away from the injury site. (g) All DMSO-treated larvae ($n = 5$ nerves in 4 larvae) demonstrated complete bridging while perineurial glia in all SB432542-treated larvae ($n = 6$ nerves in 4 larvae) failed to bridge the injury gap. (h) Schwann cells in both DMSO ($n = 4$ nerves in 3 larvae) and SB431542-treated larvae ($n = 4$ nerves in 3 larvae) did not bridge across the injury site. (i) Quantification of the timing of the first macrophage to enter the injury site in both DMSO (green, $n = 8$ nerves in 5 larvae; mean: 31.88 ± 0 min) and SB431542-treated (magenta, $n = 6$ nerves in 4 larvae; mean: 34.175.62 ± 0 min) larvae ($p = .3335$). (j) Quantification of the number of macrophages per nerve recruited to the injury site over 8 hpi in both DMSO (green, $n = 8$ nerves in 5 larvae; mean: 5.62 ± 0 macrophages) and SB431542-treated (magenta, $n = 6$ nerves in 4 larvae; mean: 4.67 ± 0 macrophages) larvae ($p = .8655$). Scale bar, (a–f) 25 μm; (a'–f'') magnified insets, 10 μm.

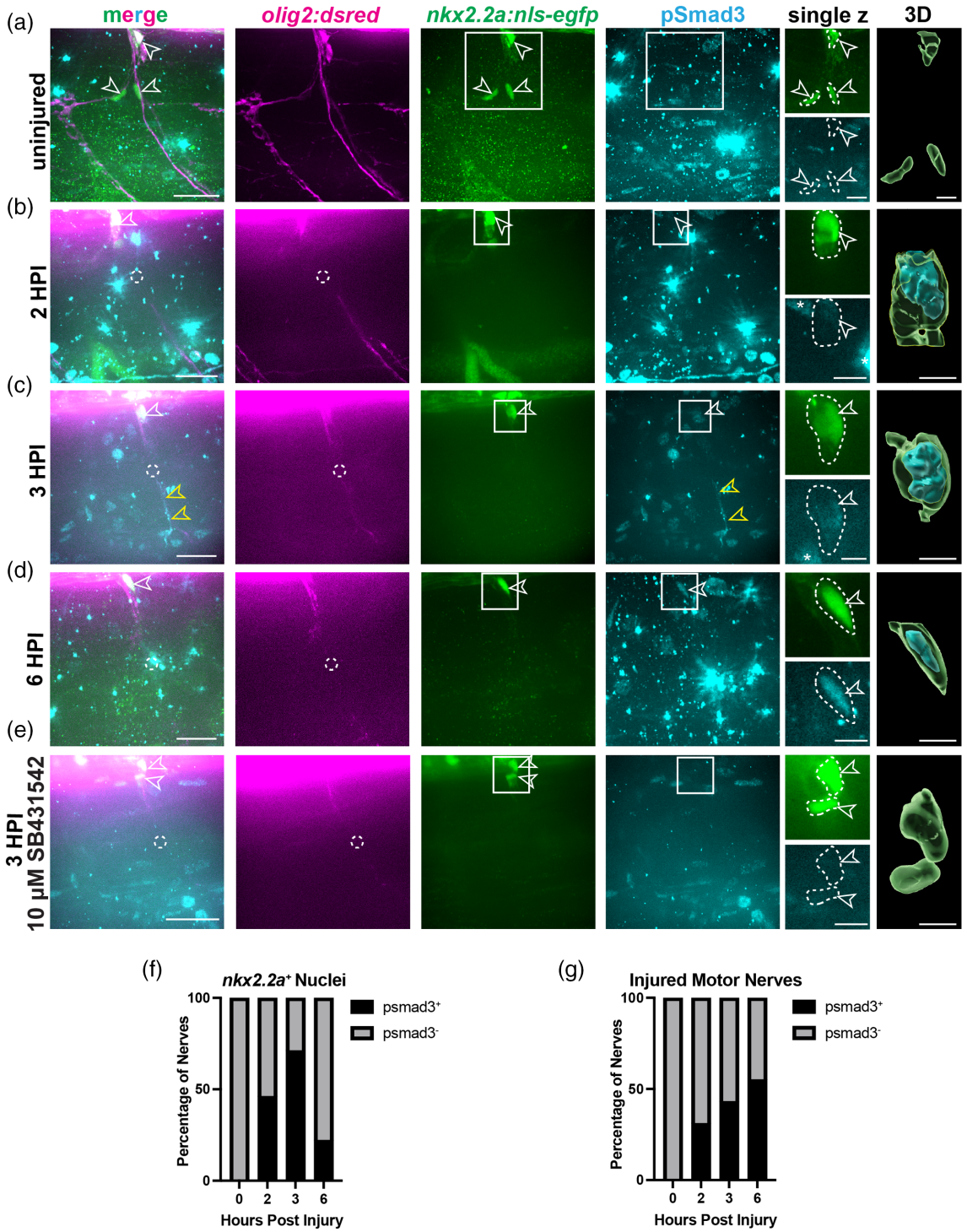

FIGURE 5 pSmad3 expression is present in perineurial glia early after injury. (a–e) Representative images of 5 or 6 dpf larvae with motor axons (magenta), *nkx2.2a*$^{+}$ nuclei (green, white open arrows), and anti-pSmad3 (cyan) in uninjured (a), 2 (b), 3 (c), 6 (d) hpi larvae, and larvae treated with SB431542 at 3 hpi (e). Anti-pSmad3 labeling is observed in *nkx2.2a*$^{+}$ nuclei (open white arrows) and along the motor nerve (open yellow arrows) at 2, 3, and 6 hpi. 6 dpf larvae treated with 10 µM SB431542 show loss of anti-pSmad3 staining at 3 hpi (bottom panels). Dashed circles indicate injury sites. Solid-line boxes indicate the area represented in enhanced single *z* planes and nuclei in 3D rendered images (Imaris). White dotted-lines outline *nkx2.2a*$^{+}$ nuclei and anti-pSmad3 labeling. (f,g) Quantification of the percentage of nerves that had anti-pSmad3^{+} labeling (black) co-localized with *nkx2.2a*$^{+}$ nuclei (f) or motor nerves (g). Chi-square tests were performed to determine significance. (f) 0% of uninjured nerves, 46% of 2 hpi nerves, 71% of 3 hpi nerves, and 22% of 6 hpi nerves had anti-pSmad3^{+} labeling in *nkx2.2a*$^{+}$ nuclei ($n = 13$ nerves in 9 larvae, 20 nerves in 4 larvae, 21 nerves in 6 larvae, 17 nerves in 4 larvae, respectively) (Chi-square: 137.7, df: 3, $p < .0001$). (g) 0% of uninjured nerves, 31% of 2 hpi nerves, 43% of 3 hpi nerves, and 55% of 6 hpi had anti-pSmad3^{+} labeling along the nerve ($n = 13$ nerves in 9 larvae, 20 nerves in 4 larvae, 21 nerves in 6 larvae, 17 nerves in 4 larvae, respectively) (Chi-square: 63.92, df: 3, $p < .0001$). Scale bars, 25 µm; magnified insets, 10 µm; 3D renderings, 5 µm.

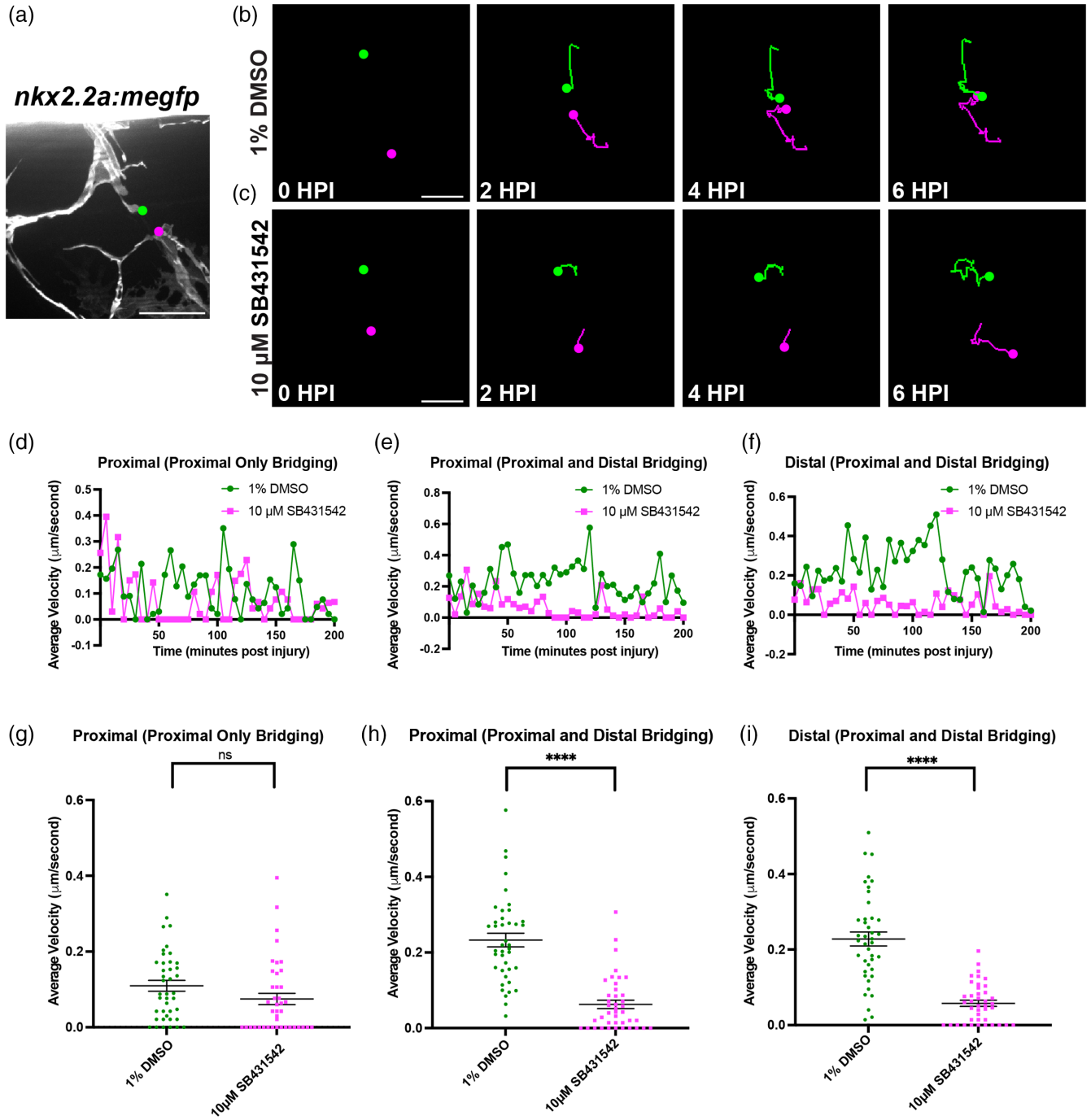

FIGURE 6 Inhibition of TGFβ signaling alters perineurial glial bridging dynamics. (a) Representative image of a recently transected spinal motor nerve in a 6 dpf *nkx2.2a:megfp* larva with the proximal (green dot) and distal (magenta dot) stumps labeled. (b,c) Representative images from tracking of both the proximal (green dot) and distal (magenta dot) stumps from time-lapse movies of perineurial glia in injured 5 or 6 dpf larvae treated with either 1% DMSO (b) or 10 µM SB431542 (c). (d–i) Quantification of the average velocity of perineurial glial membrane proximal or distal stumps in µm/s plotted over time (d–f) or for the first 200 min post injury (mpi) (g–i). Velocities were calculated every 5 min using FIJI. Each dot represents the average velocity of all larvae within a group at that specific time point. (d,g) There is no significant difference in proximal only perineurial glial bridging velocity between DMSO and SB431542-treated larvae (mean: 0.116 ± 0.02 µm/s, 0.063 ± 0.015 µm/s, respectively; $p = .1078$) ($n = 3$ nerves in 3 larvae, $n = 3$ nerves in 3 larvae, respectively). (e,f,h,i) There is a significant difference in perineurial glial bridging velocity between DMSO and SB432542-treated larvae, with DMSO-treated larvae having a higher average velocity, ($n = 4$ nerves in 3 larvae, $n = 3$ nerves in 3 larvae, respectively) in both proximal (mean: 0.139 ± 0.03, 0.08 ± 0.02 µm/s, respectively; $p < .0001$) and proximal and distal (mean: 0.18 ± 0.03, 0.06 ± 0.02 µm/s; $p < .0001$) bridging in larvae that had bridging from both the proximal and distal perineurial glial ends. Scale bars, (a) 25 µm; (b,c) tracking images, 10 µm.

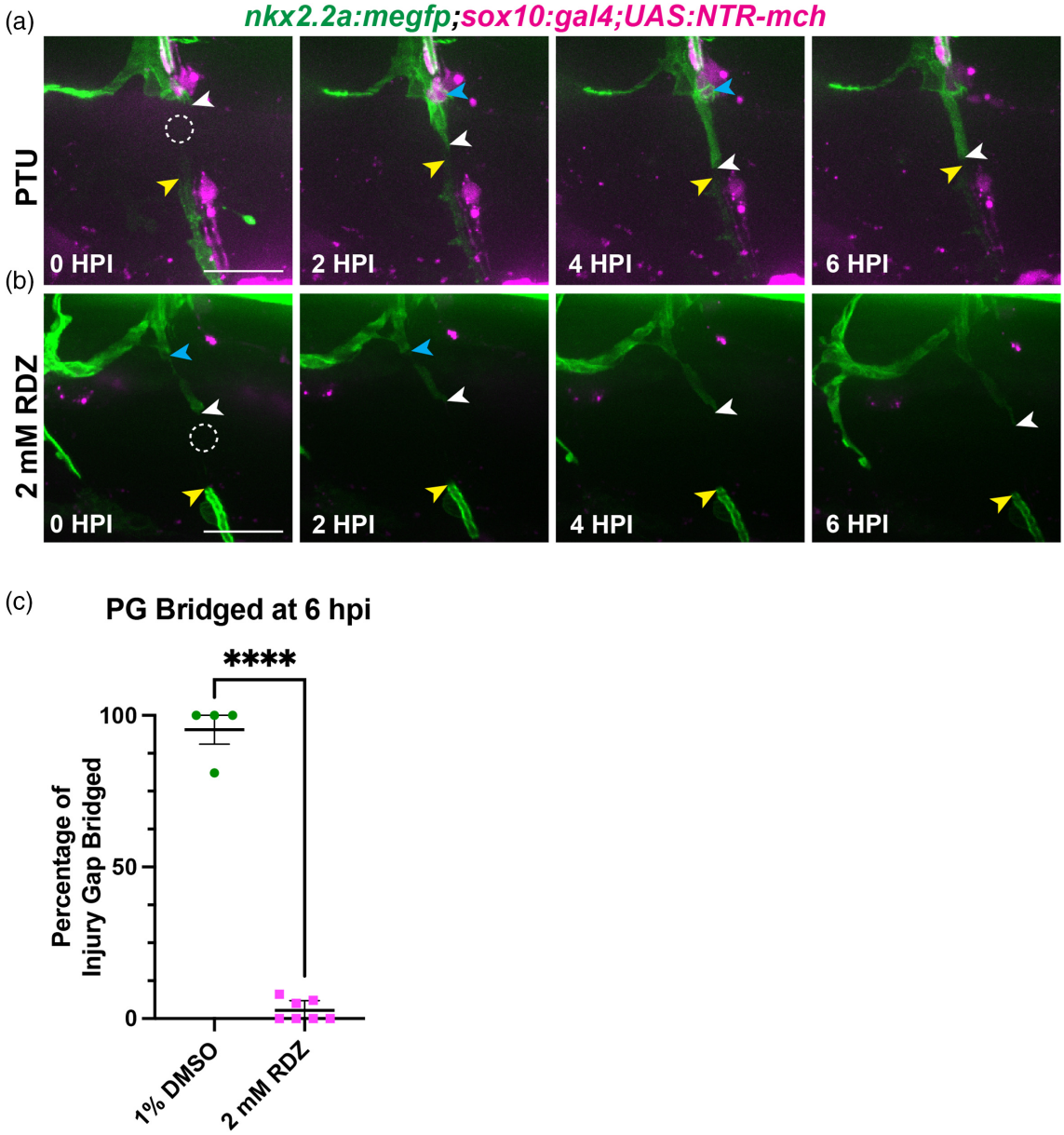

FIGURE 7 Elimination of Schwann cells immediately prior to injury perturbs perineurial glial bridging. (a,b) Representative images from stills of time-lapse movies of injured 5 or 6 dpf *nkx2.2a:megfp;sox10:gal4;UAS:NTR-mch* larvae. Dashed circles indicate injury sites. White arrows follow the proximal end and yellow arrows follow the distal end of the perineurial glial bridge (green). Blue arrows indicate phagocytic vesicles. Larvae were treated with either (a) PTU egg water ($n = 4$ nerves in 3 larvae) or (b) 2 mM ronidazole (RDZ) in PTU egg water ($n = 7$ nerves in 5 larvae). (c) Quantification of the percentage of the injury gap bridged by perineurial glia (PG) at 6 hpi in larvae treated with either PTU water (green, $n = 4$ nerves in 3 larvae; mean: 95.25 ± 1.32) or 2 mM RDZ (magenta, $n = 7$ nerves in 5 larvae; mean: 2.71 ± 1.32) ($p < .0001$;). Scale bar, 25 μm.

stained all groups with an antibody specific to pSmad3. In these studies, using Imaris (Oxford Instruments) to render 3D images of *nkx2.2a*$^{+}$ nuclei and pSmad3 signal, we observed pSmad3-positive *nkx2.2a*$^{+}$ nuclei in both *ctgfa*$^{+/+}$ and *ctgfa*$^{+/-}$ larvae (Figure 10a,b,d; $n = 52$ nerves in 10 larvae, 20 nerves in 7 larvae, respectively). However, we did not observe pSmad3-positive *nkx2.2a*$^{+}$ nuclei in *ctgfa*$^{-/-}$ larvae (Figure 10c,d; $n = 23$ nerves in 6 larvae). Similarly, we observed pSmad3 labeling along motor nerves in some *ctgfa*$^{+/+}$ and *ctgfa*$^{+/-}$ larvae, with no pSmad3 labeling along motor nerves in *ctgfa*$^{-/-}$ larvae (Figure 10e; $n = 52$ nerves in 10 larvae, 20 nerves in 7 larvae, $n = 23$ nerves in 6 larvae, respectively). This loss of pSmad3 labeling in *nkx2.2a*$^{+}$ nuclei and along the nerve after injury only in *ctgfa*$^{-/-}$ larvae indicates that perineurial glia lose TGFβ signaling, and subsequently an ability to bridge, as a result of a loss of *ctgfa* expression, suggesting that these two signals do indeed work in a positive feedback loop to drive perineurial glial bridging.

Based on our data, we propose a model in which TGFβ signaling and *ctgfa* work in a positive feedback loop to drive perineurial glial bridging (Figure 11). Our data shows that perineurial glia independently require TGFβ signaling (Figure 3d), the presence of Schwann

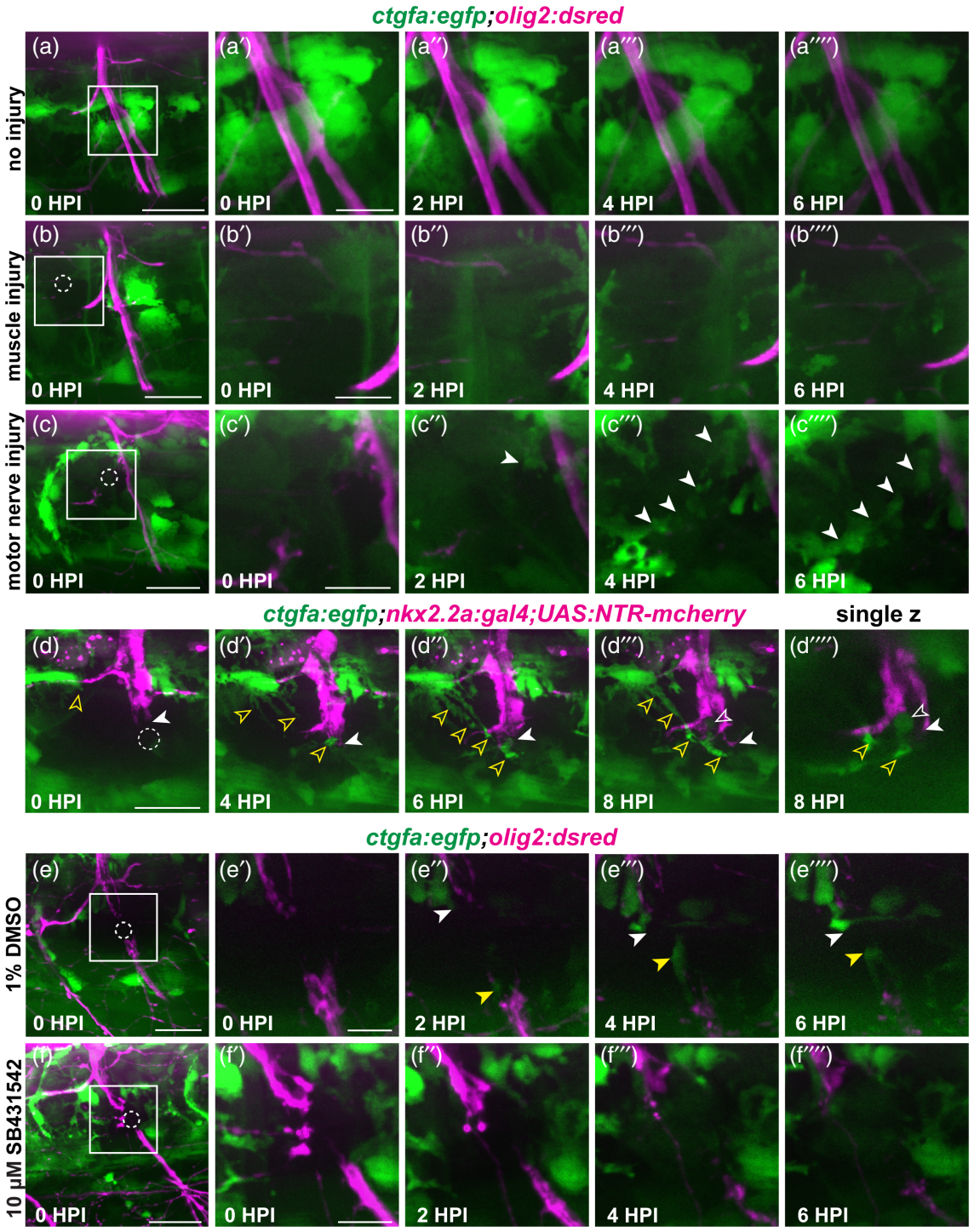

FIGURE 8 *ctgfa* expression increases at the injury site. (a–c) Representative images from stills of time-lapse movies of 5 or 6 dpf *ctgfa:egfp*; *olig2:dsred* larvae. Larvae were either uninjured (a; $n = 4$ nerves in 4 larvae), injured in muscle adjacent to spinal motor nerves (b; $n = 4$ nerves in 4 larvae), or injured along the spinal motor nerve (c; $n = 11$ nerves in 5 larvae) and time-lapse imaged for 6 hpi. Dashed circles indicate the injury site. White arrows indicate increased *ctgfa* expression. (d) Representative images from stills of a time-lapse movie of a 6 dpf *nkx2.2a:gal4;UAS:NTR-mcherry;ctgfa:egfp* larva ($n = 6$ nerves in 4 larvae). A single *z*-plane image demonstrates potential regions of co-localization of perineurial glia (magenta) and *ctgfa* expression (green) at 8 hpi. Solid white arrows follow bridging perineurial glia across the injury site. Open white arrows indicate *ctgfa* expression that might co-localize with perineurial glia. Open yellow arrows specify increased *ctgfa* expression that does not co-localize with perineurial glia. (e,f) Representative images from stills of time-lapse movies of 5 or 6 dpf *ctgfa:egfp;olig2:dsred* larvae. Larvae were either treated with 1% DMSO (E; $n = 4$ nerves in 3 larvae) or 10 µM SB431542 (F; $n = 4$ nerves in 3 larvae). White arrows follow the increase in *ctgfa* expression proximal to the injury site and yellow arrows follow the increase in *ctgfa* distal to the injury site. Scale bars, 25 µm; magnified insets, 10 µm.

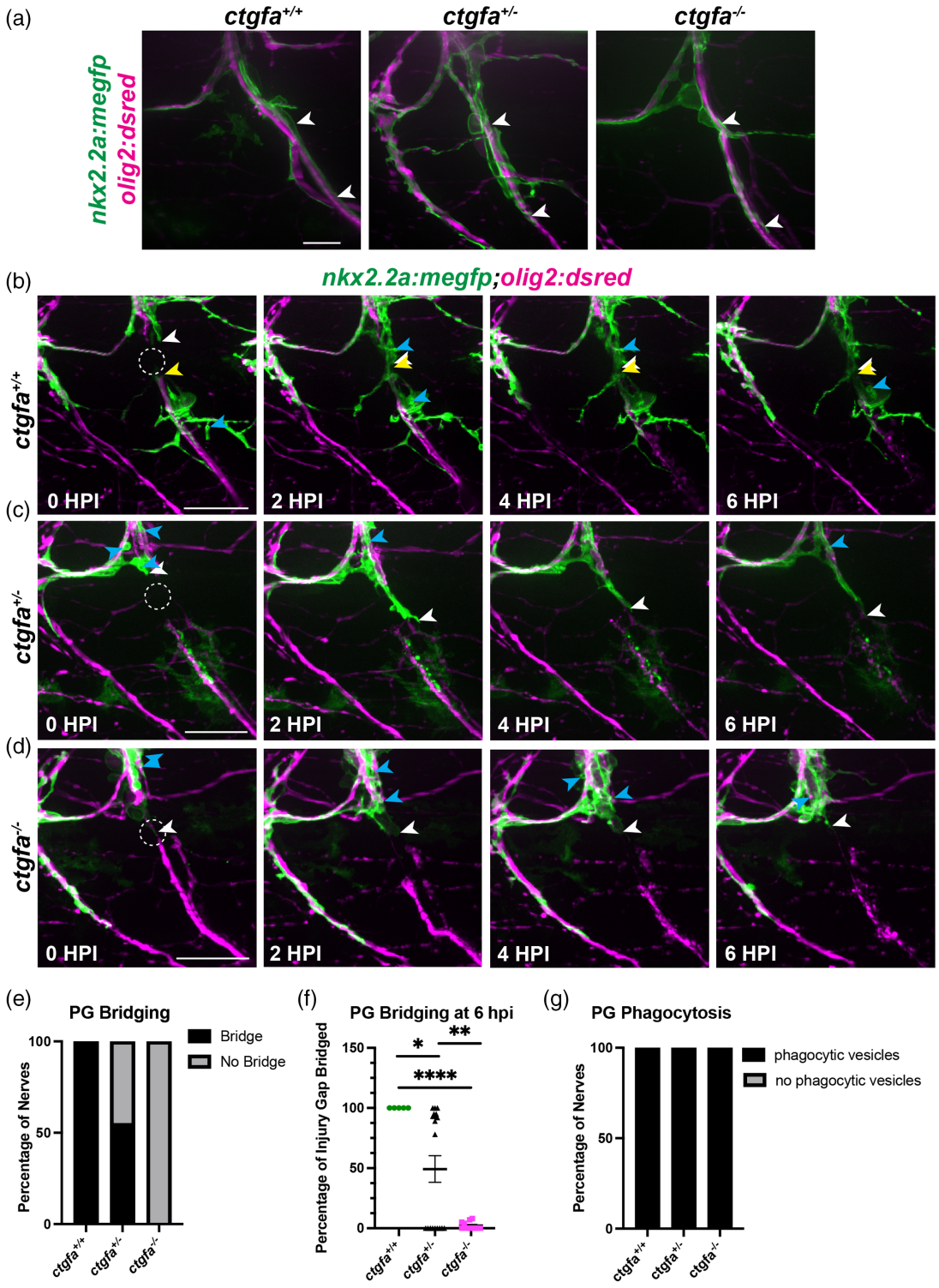

FIGURE 9 Perineurial glial bridging is perturbed in *ctgfa* mutants. (a) Representative images prior to injury of 5 dpf *ctgfa*$^{+/+}$, *ctgfa*$^{+/-}$, and *ctgfa*$^{-/-}$ *nkx2.2a:megfp;olig2:dsred* larvae. White arrows indicate healthy perineurial glia fully ensheathing motor nerves. (b–d) 5 or 6 dpf larvae with *ctgfa*$^{+/+}$ ($n = 5$ nerves in 4 larvae), *ctgfa*$^{+/-}$ ($n = 19$ nerves in 10 larvae), or *ctgfa*$^{-/-}$ ($n = 11$ nerves in 6 larvae) genotypes. (b–d) Representative images from time-lapse movies of 5 or 6 dpf *ctgfa*$^{+/+}$ (b), *ctgfa*$^{+/-}$ (c), or *ctgfa*$^{-/-}$ (d) larvae where spinal motor nerves were injured. Dashed circles indicate injury site. White arrows follow the proximal end and yellow arrows follow the distal end of the perineurial glial bridge. Blue arrows specify perineurial glial phagocytic vesicles. (e) Quantification of percentage of nerves in which perineurial glia bridged (black) or did not bridge (gray) across *ctgfa*$^{+/+}$, *ctgfa*$^{+/-}$, or *ctgfa*$^{-/-}$ genotypes. (f) Quantification of the percentage of the injury gap bridged by perineurial glia at 6 hpi by *ctgfa*$^{+/+}$, *ctgfa*$^{+/-}$, or *ctgfa*$^{-/-}$ larvae (mean ± SEM: *ctgfa*$^{+/+}$: 100 ± 0; *ctgfa*$^{+/-}$: 49.21 ± 11.06; *ctgfa*$^{-/-}$: 2.18 ± 0.96. *p* values: *ctgfa*$^{+/+}$ vs. *ctgfa*$^{+/-}$: $p = .0301$; *ctgfa*$^{+/+}$ vs. *ctgfa*$^{-/-}$: $p < .0001$; *ctgfa*$^{+/-}$ vs. *ctgfa*$^{-/-}$: $p = .0033$). (g) Quantification of presence of phagocytic vesicles in *ctgfa*$^{+/+}$, *ctgfa*$^{+/-}$, or *ctgfa*$^{-/-}$ larvae. Phagocytic vesicles were present in 100% of larvae across all genotypes. Scale bars, (a) pre-injury images, 10 μm; (b–d) 25 μm.

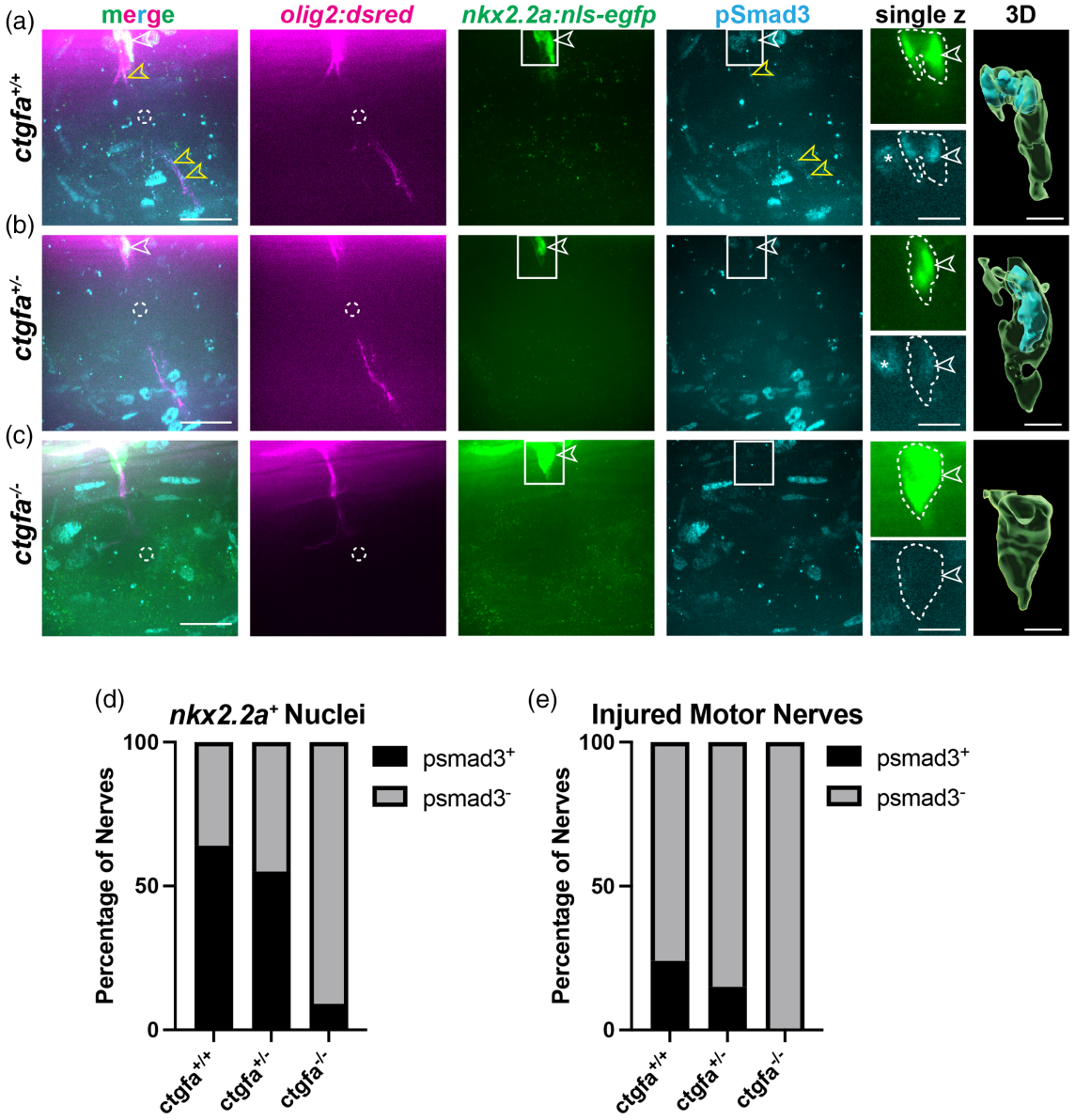

FIGURE 10 pSmad3 expression is absent in *nkx2.2a*$^{+}$ nuclei in *ctgfa* mutants. (a–c) Representative images of 5 or 6 dpf larvae with motor axons (magenta), *nkx2.2a*$^{+}$ nuclei (green), and anti-pSmad3 (cyan) in *ctgfa*$^{+/+}$ (a), *ctgfa*$^{+/-}$ (b), and *ctgfa*$^{-/-}$ (c) larvae at 3 hpi. Anti-pSmad3 labeling is observed in *nkx2.2a*$^{+}$ nuclei (open white arrows) and along the motor nerve (open yellow arrows) in *ctgfa*$^{+/+}$ and some *ctgfa*$^{+/-}$ larvae. *ctgfa*$^{-/-}$ larvae show loss of anti-pSmad3 staining in *nkx2.2a*$^{+}$ nuclei at 3 hpi. Dashed circles indicate injury sites. Solid-line boxes indicate the area represented in enhanced single *z* planes and nuclei in 3D rendered images (Imaris). White dotted-lines outline *nkx2.2a*$^{+}$ nuclei and anti-pSmad3 labeling. (d,e) Quantification of the percentage of nerves that had anti-pSmad3^{+} labeling (black) co-localized with *nkx2.2a*$^{+}$ nuclei (d) or motor nerves (e). Chi-square tests were performed to determine significance (*ctgfa*$^{+/+}$: $n = 52$ nerves in 10 larvae, *ctgfa*$^{+/-}$: $n = 20$ nerves in 7 larvae, *ctgfa*$^{-/-}$: $n = 23$ nerves in 6 larvae). (d) 64% of *ctgfa*$^{+/+}$ nerves, 55% of *ctgfa*$^{+/-}$ nerves, and 9% of *ctgfa*$^{-/-}$ nerves had anti-pSmad3^{+} labeling in *nkx2.2a*$^{+}$ nuclei (Chi-square: 71.16, df: 2, $p < .0001$). (e) 24% of *ctgfa*$^{+/+}$ nerves, 15% of *ctgfa*$^{+/-}$ nerves, and 0% of *ctgfa*$^{-/-}$ nerves had anti-pSmad3^{+} labeling in *nkx2.2a*$^{+}$ nuclei (Chi-square: 25.99, df: 2, $p < .0001$). Scale bars, 25 μm; magnified insets, 10 μm; 3D renderings, 5 μm.

cells (Figure 7b), and *ctgfa* signaling (Figure 9d) for bridging following spinal motor nerve injury. Additionally, inhibition of TGFβ signaling leads to a loss of *ctgfa* expression in the injury site after injury (Figure 8f) while absence of *ctgfa* expression leads to a loss of pSmad3 expression in *nkx2.2a*$^{+}$ nuclei 3 hpi after injury (Figure 10c). Therefore, we hypothesize that following spinal motor nerve injury, TGFβ signaling, potentially derived from Schwann cells, drives an increase in *ctgfa* expression. This increase in *ctgfa* expression then in turn stimulates binding of TGFβ-1 to its receptors to drive the TGFβ signaling necessary for perineurial glial bridging. It is possible that the stimulation of TGFβ signaling by *ctgfa* is necessary to initiate perineurial glial bridging, and that basal availability of TGFβ signaling is insufficient to do so. Therefore, loss of TGFβ signaling would cause a loss of both perineurial glial bridging (Figure 3d) and *ctgfa* expression (Figure 9d)

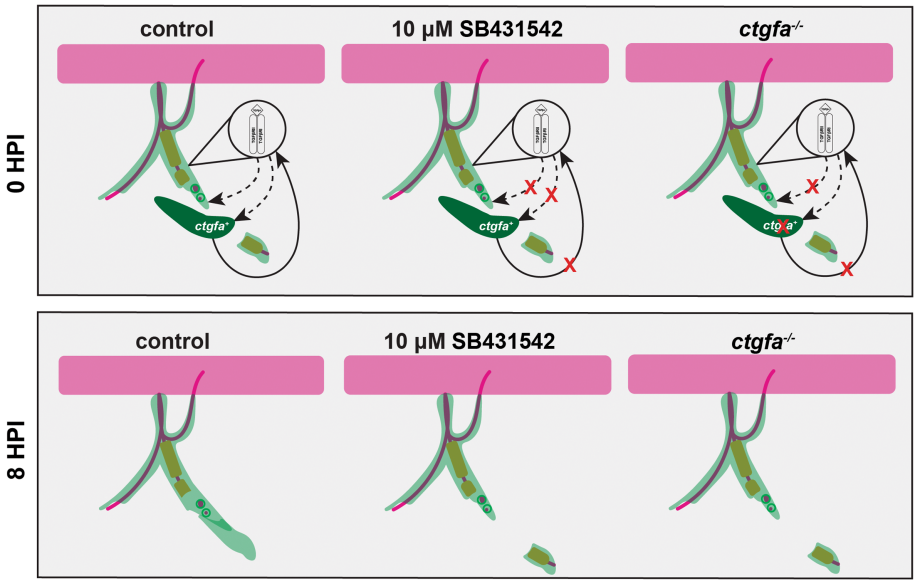

FIGURE 11 Perineurial glial bridging is modulated by a positive feedback loop between TGFβ signaling and *ctgfa*. Summary diagram of our proposed signaling model that drives perineurial glial bridging after injury in control, 10 μM SB431542, and *ctgfa*$^{-/-}$ conditions at 0 (top panels) and 8 hpi (bottom panels). Motor axons (magenta), Schwann cells (orange), perineurial glia (light green), *ctgfa* expressing cells (dark green). The magnified region designates perineurial glial-specific TGFβ signaling. Dotted-lines indicate TGFβ signaling whereas solid lines indicate *ctgfa* signaling. Red "X"s demonstrate pathways that are inhibited or turned off in either 10 μM SB431542 treatment or *ctgfa*$^{-/-}$ larvae.

after injury, as observed with our SB431542-treated larvae (Figure 11). Subsequently, loss of *ctgfa* expression would cause a loss of perineurial glial bridging (Figure 9d) due to insufficient availability of TGFβ signaling, as observed in our *ctgfa*$^{-/-}$ larvae (Figure 11). Further, pSmad3 antibody staining is lost in *nkx2.2a*$^{+}$ nuclei in *ctgfa*$^{-/-}$ larvae at 3 hpi (Figure 10c), confirming that *ctgfa* and TGFβ signaling are indeed working together to initiate perineurial glial bridging. Therefore, we conclude that TGFβ signaling drives perineurial glial bridging after spinal motor nerve injury through a positive feedback loop with *ctgfa*.

4 | DISCUSSION

Understanding the cellular and molecular drivers of peripheral motor nerve regeneration is crucial to gaining insight into effective and functional recovery after injury. Most research focuses on the roles that Schwann cells and macrophages play in regeneration (Chen et al., 2015; Chen et al., 2021; Clements et al., 2017; Jessen & Mirsky, 2019; Rosenberg et al., 2012; Schira et al., 2018). However, we know that perineurial glia are also essential for efficient nerve regeneration (Lewis & Kucenas, 2014). Here, we show that TGFβ signaling drives perineurial glial bridging. We also introduce a factor downstream of TGFβ signaling, *ctgfa*, which is necessary for perineurial bridging. These data unlock novel insights into what drives perineurial glial bridging, a process that is essential for successful nerve regeneration.

4.1 | TGFβ signaling drives perineurial glial bridging after spinal motor nerve injury

Perineurial glia are one of the first cell types to respond to spinal motor nerve injury in zebrafish and initiate the regeneration process by phagocytosing debris and bridging across the injury site within the first 8 hpi (Lewis & Kucenas, 2014). Our data demonstrates that the location of perineurial glial nuclei relative to the injury site influences whether perineurial glia bridge from both the proximal and distal side of the injury or just from the proximal side. While the location of perineurial glial nuclei affects the type of bridging that occurs, it is also likely that location of perineurial glial nuclei could affect signaling that occurs during bridging. Following the inhibition of TGFβ signaling, perineurial glial proximal stump velocity is decreased relative to DMSO-treated larvae along nerves that had proximal and distal bridging. However, proximal stump velocity is not decreased relative to DMSO-treated controls along nerves that had proximal only bridging. This data raises the possibility that TGFβ signaling might be acting in a paracrine manner in perineurial glia, and that the lack of distal perineurial glia in proximal only bridging nerves might result in a smaller source of TGFβ signaling in DMSO-treated control larvae, causing their initial velocity to be more similar to that of those with TGFβ inhibition. Therefore, the availability of TGFβ signaling depending on the position of perineurial glial nuclei relative to the injury site might influence the ability of perineurial glia to initiate bridging.

Alternatively, it is possible that TGFβ signaling indirectly drives perineurial glial bridging. Previous studies demonstrate that perineurial glial fail to bridge but continue to phagocytose debris in the absence of Schwann cells (Lewis & Kucenas, 2014). TGFβ-1 is secreted from Schwann cells after injury and is necessary for their transformation from myelinating into repair Schwann cells (Clements et al., 2017; Schira et al., 2018). Perineurial glial bridge before Schwann cells form bands of Bungner and physically enter the injury site (Lewis & Kucenas, 2014). Our studies demonstrate that when Schwann cells are present during development but eliminated immediately prior to injury, perineurial glia are unable to bridge. Therefore, it is possible that perineurial glia are bridging during the time in which Schwann cells secrete TGFβ-1. For this reason, Schwann cells are another potential

source of TGFβ-1. Future studies further investigating the source of TGFβ-1 and whether this signaling is directly or indirectly affecting perineurial glial bridging will shed light on this possibility.

Finally, our studies demonstrate that pSmad3 is present in *nkx2.2a*$^{+}$ nuclei early during perineurial glial bridging behaviors, peaking at about 3 hpi, suggesting that TGFβ signaling in perineurial glia is important for the initiation of bridging. Although we know TGFβ signaling is crucial for the initiation of bridging, we do not know if acute or sustained inhibition of this cascade is what causes this phenotype. Further understanding the critical period of TGFβ signaling required for perineurial glial bridging could provide insight into what cells might be a direct source of this molecule and reveal potential therapeutic targets for enhancing peripheral nerve regeneration.

4.2 | Perineurial glial bridging and phagocytosis are controlled by separate molecular mediators

In addition to bridging, perineurial glia phagocytose debris after injury. Consistent with previous work from our lab, we observed that perineurial glial phagocytosis is more prominent on the proximal stump than on the distal stump (Lewis & Kucenas, 2014). In the absence of Schwann cells, perineurial glia fail to bridge, however they continue to phagocytose debris (Lewis & Kucenas, 2014). Our data demonstrates that while perineurial glia fail to bridge in the absence of TGFβ signaling, elimination of Schwann cells, or depletion of *ctgfa* expression, they continue to phagocytose debris, supporting the hypothesis that perineurial glial bridging and phagocytosis are controlled by distinct molecular drivers. Further, perineurial glia do not appear to phagocytose Schwann cell debris, suggesting that perineurial glial phagocytosis is specific to axonal debris and supporting previous work demonstrating that perineurial glia, Schwann cells, and macrophages spatially coordinate to clear debris after injury. Future studies aiming to identify potential signaling pathways that control perineurial glial phagocytosis would add to our understanding of the full molecular repertoire that drives the perineurial glial injury response. Such studies could also elucidate the role that perineurial glial phagocytosis plays in debris clearance and whether their phagocytosis is required for perineurial glial bridging as well as full regeneration. Because perineurial glia phagocytose axonal debris primarily on the proximal stump of the axon, it is possible that without perineurial glial phagocytosis clearing debris to create a growth permissive environment, perineurial glia would not be able to establish a bridge.

4.3 | Connective tissue growth factor-a is necessary for perineurial glial bridging

ctgfa is a well-known driver of regenerative responses after injury (Mokalled et al., 2016; Mukherjee et al., 2021). Additionally, *ctgfa* works in a positive feedback loop with TGFβ signaling to increase the production of TGFβ-1 (Abreu et al., 2002). Our results support the presence of this feedback loop, as inhibition of TGFβ signaling resulted in a loss of *ctgfa* expression after injury. Similarly, absence of *ctgfa* signaling in *ctgfa* mutants phenocopied the loss of TGFβ signaling, with both resulting in the loss of perineurial glial bridging but the retention of perineurial glial phagocytosis and the loss of pSmad3 staining in *nkx2.2a*$^{+}$ nuclei at 3 hpi. This suggests that loss of *ctgfa* expression might be affecting TGFβ signaling levels, therefore indirectly affecting perineurial glial bridging through the downregulation of TGFβ signaling.

In our imaging with *ctgfa:egfp* after injury, we observed expression of *ctgfa* increase in the injury site during the first 6 hpi, the period during which perineurial glia are forming their bridge. While CTGF is secreted by Schwann cells after injury (Schira et al., 2018), we see an increase in *ctgfa* expression in the injury site in the first 6 hpi, before Schwann cells migrate into the injury site and form Bands of Bungner. Therefore, it is unlikely that the cells we observe expressing *ctgfa* during this time are Schwann cells. Perineurial glia express *ctgfa* during development (data not shown), therefore it is possible that perineurial glia express *ctgfa* during regeneration. Although we do not observe co-localization of *ctgfa* expression with perineurial glia during the first 8 hpi, it is still possible that perineurial glia are expressing *ctgfa* at a low level that is difficult to observe with the tools currently available. Additionally, we observed cells that express *ctgfa* actively respond to motor nerve injury but are not physically found along the nerve. Therefore, additional cells are expressing *ctgfa* as a response to injury, and these cells could be indirectly driving perineurial glial bridging through *ctgfa* expression and enhancement of TGFβ signaling. It is likely that TGFβ signaling, potentially derived from Schwann cells, alone is insufficient to drive perineurial glial bridging, and enhancement of this basal TGFβ signaling by *ctgfa* expression is sufficient to drive bridging. This is supported by our data, where eliminating TGFβ signaling, the presence of Schwann cells, or *ctgfa* expression independently produced similar phenotypes, with perineurial glia unable to form a bridge but continuing to phagocytose debris. Future studies investigating which cells are expressing *ctgfa* after injury and the role that these cells play in perineurial glial bridging and motor nerve regeneration will be key to closing this loop. These cells could be epineurium or endoneurium cells, of which little is known about their injury responses and of which we currently lack specific markers. Further, perineurial glia act as a component of the blood-nerve barrier in both mice and zebrafish (Clark et al., 2014; Kucenas, Takada, et al., 2008) and *ctgfa* is important for angiogenesis during wound healing (Abreu et al., 2002; Schira et al., 2018). Therefore, *ctgfa* could be driving perineurial glial bridging through stimulation of TGFβ signaling while concurrently aiding in reinnervation of vasculature following injury, with endothelial cells being the *ctgfa*$^{+}$ cells we observe. Future studies investigating the relationship between blood vessel bridging and perineurial glial bridging are important to determine the role that perineurial glia play in reinnervation following injury.

Together, our work establishes TGFβ signaling as an essential driver of perineurial glial bridging after peripheral motor nerve injury in zebrafish. We found that TGFβ signaling is important for early

initiation of perineurial glial bridging. Further, we identify *ctgfa* as a downstream effector of TGFβ signaling that is necessary for perineurial glial bridging. Although both TGFβ and *ctgfa* signaling are known to be involved in peripheral nerve regeneration and wound healing (Clements et al., 2017; Mokalled et al., 2016; Mukherjee et al., 2021; Schira et al., 2018; Sulaiman & Nguyen, 2016), this work highlights a novel and crucial role for both of these signals in the perineurial glial injury response. Collectively, these studies increase our understanding of how perineurial glial respond to injury and provide insight into potential cellular and molecular targets for therapeutics to enhance and promote regeneration.

AUTHOR CONTRIBUTIONS

Conceptualization: Kimberly A. Arena and Sarah Kucenas; Methodology: Kimberly A. Arena, Yunlu Zhu, and Sarah Kucenas; Formal Analysis: Kimberly A. Arena; Investigation: Kimberly A. Arena and Sarah Kucenas; Writing: Kimberly A. Arena and Sarah Kucenas; Funding Acquisition: Kimberly A. Arena and Sarah Kucenas.

ACKNOWLEDGMENTS

This work was funded by the Jefferson Scholars Foundation (KAA) and the National Institutes of Health (NIH): NS107525 (SK) and T32GM008136 (KAA). We would like to thank members of the Kucenas Lab, past and present, for valuable discussions, Lori Tocke for zebrafish care, and Dr. Mayssa Mokalled for generously gifting us the *ctgfa*:*egfp* and *ctgfa* mutant fish lines.

CONFLICT OF INTEREST

The authors have no competing interests to report.

DATA AVAILABILITY STATEMENT

The data that support the findings of this study are available from the corresponding author upon reasonable request.

ORCID

Sarah Kucenas https://orcid.org/0000-0002-1950-751X

REFERENCES

Abarca-Buis, R. F., Mandujano-Tinoco, E. A., Cabrera-Wrooman, A., & Krötzsch, E. (2021). The complexity of TGFβ/activin signaling in regeneration. *Journal of Cell Communication and Signaling*, *15*(1), 7–23. https://doi.org/10.1007/s12079-021-00605-7

Abreu, J. G., Ketpura, N. I., Reversade, B., & De Robertis, E. M. (2002). Connective-tissue growth factor (CTGF) modulates cell signalling by bmp and TGF-β. *Nature Cell Biology*, *4*, 599–604. https://doi.org/10.1038/ncb826

Balakrishnan, A., Belfiore, L., Chu, T. H., Fleming, T., Midha, R., Biernaskie, J., & Schuurmans, C. (2021). Insights into the role and potential of Schwann cells for peripheral nerve repair from studies of development and injury. *Frontiers in Molecular Neuroscience*, *13*, 270. https://doi.org/10.3389/fnmol.2020.608442

Behrman, J. E., & Acland, R. D. (1981). Experimental study of the regenerative potential of perineurium at a site of nerve transection. *Journal of Neurosurgery*, *54*(1), 79–83. https://doi.org/10.3171/jns.1981.54.1.0079

Binari, L. A., Lewis, G. M., & Kucenas, S. (2013). Perineurial glia require notch signaling during motor nerve development but not regeneration. *Journal of Neuroscience*, *33*(10), 4241–4252. https://doi.org/10.1523/jneurosci.4893-12.2013

Brosius Lutz, A., Lucas, T. A., Carson, G. A., Caneda, C., Zhou, L., Barres, B. A., Buckwalter, M. S., & Sloan, S. A. (2022). An RNA-sequencing transcriptome of the rodent Schwann cell response to peripheral nerve injury. *Journal of Neuroinflammation*, *19*(1), 105. https://doi.org/10.1186/S12974-022-02462-6

Casari, A., Schiavone, M., Facchinello, N., Vettori, A., Meyer, D., Tiso, N., Moro, E., & Argenton, F. (2014). A Smad3 transgenic reporter reveals TGF-beta control of zebrafish spinal cord development. *Developmental Biology*, *396*(1), 81–93. https://doi.org/10.1016/j.ydbio.2014.09.025

Cattin, A. L., & Lloyd, A. C. (2016). The multicellular complexity of peripheral nerve regeneration. *Current Opinion in Neurobiology*, *39*, 38–46. https://doi.org/10.1016/j.conb.2016.04.005

Chen, B., Banton, M. C., Singh, L., Parkinson, D. B., & Dun, X. P. (2021). Single cell transcriptome data analysis defines the heterogeneity of peripheral nerve cells in homeostasis and regeneration. *Frontiers in Cellular Neuroscience*, *15*, 1–22. https://doi.org/10.3389/fncel.2021.624826

Chen, P., Piao, X., & Bonaldo, P. (2015). Role of macrophages in Wallerian degeneration and axonal regeneration after peripheral nerve injury. *Acta Neuropathologica*, *130*(5), 605–618. https://doi.org/10.1007/s00401-015-1482-4

Clark, J. K., O'keefe, A., Mastracci, T. L., Sussel, L., Matise, M. P., & Kucenas, S. (2014). Mammalian Nkx2.2+ perineurial glia are essential for motor nerve development. *Developmental Dynamics*, *243*(9), 1116–1129. https://doi.org/10.1002/dvdy.24158

Clements, M. P., Byrne, E., Camarillo Guerrero, L. F., Cattin, A. L., Zakka, L., Ashraf, A., Burden, J. J., Khadayate, S., Lloyd, A. C., Marguerat, S., & Parrinello, S. (2017). The wound microenvironment reprograms Schwann cells to invasive mesenchymal-like cells to drive peripheral nerve regeneration. *Neuron*, *96*(1), 98–114. https://doi.org/10.1016/j.neuron.2017.09.008

Coleman, M. P., & Freeman, M. R. (2010). Wallerian degeneration, Wld^S, and Nmnat. *Annual Review of Neuroscience*, *33*(1), 245–267. https://doi.org/10.1146/annurev-neuro-060909-153248

Das, A., & Crump, J. G. (2012). Bmps and Id2a act upstream of Twist1 to restrict ectomesenchyme potential of the cranial neural crest. *PLoS Genetics*, *8*(5), e1002710. https://doi.org/10.1371/JOURNAL.PGEN.1002710

D'Rozario, M., Monk, K. R., & Petersen, S. C. (2017). Analysis of myelinated axon formation in zebrafish. *Methods in Cell Biology*, *138*, 383–414. https://doi.org/10.1016/bs.mcb.2016.08.001

Dutton, K. A., Pauliny, A., Lopes, S. S., Elworthy, S., Carney, T. J., Rauch, J., Geisler, R., Haffter, P., & Kelsh, R. N. (2001). Zebrafish colourless encodes sox10 and specifies non-ectomesenchymal neural crest fates. *Development*, *128*(21), 4113–4125.

Ellett, F., Pase, L., Hayman, J. W., Andrianopoulos, A., & Lieschke, G. J. (2011). *mpeg1* promoter transgenes direct macrophage-lineage expression in zebrafish. *Blood*, *117*(4), 49–56. https://doi.org/10.1182/blood-2010-10-314120

Fernandez, C., Iyer, M., & Low, I. (2017). Gpr126 is critical for Schwann cell function during peripheral nerve regeneration. *The Journal of Neuroscience*, *37*(12), 3106–3108. https://doi.org/10.1523/jneurosci.0127-17.2017

Fontenas, L., & Kucenas, S. (2021). Spinal cord precursors utilize neural crest cell mechanisms to generate hybrid peripheral myelinating glia. *eLife*, *10*, 1–34. https://doi.org/10.7554/eLife.64267

Frostick, S. P., Yin, Q., & Kemp, G. J. (1998). Schwann cells, neurotrophic factors, and peripheral nerve regeneration. *Microsurgery*, *18*(7), 397–405. https://doi.org/10.1002/(SICI)1098-2752(1998)18:7<397::AID-MICR2>3.0.CO;2-F

Ghosh, S., & Hui, S. P. (2016). Regeneration of zebrafish CNS: Adult neurogenesis. *Neural Plasticity*, *2016*, 1–21. https://doi.org/10.1155/2016/5815439

Gonzalez, D., & Allende, M. L. (2021). Current advances in comprehending dynamics of regenerating axons and axon–glia interactions after peripheral nerve injury in zebrafish. *International Journal of Molecular Sciences*, *22*(5), 1–11. https://doi.org/10.3390/ijms22052484

Huebner, E. A., & Strittmatter, S. M. (2009). Axon regeneration in the peripheral and central nervous systems. *Results and Problems in Cell Differentiation*, *48*, 339–351. https://doi.org/10.1007/400_2009_19

Jessen, K. R., & Mirsky, R. (2005). The origin and development of glial cells in peripheral nerves. *Nature Reviews. Neuroscience*, *6*, 671–682. https://doi.org/10.1038/nrn1746

Jessen, K. R., & Mirsky, R. (2016). The repair Schwann cell and its function in regenerating nerves. *The Journal of Physiology*, *13*, 3521–3531. https://doi.org/10.1113/JP270874

Jessen, K. R., & Mirsky, R. (2019). The success and failure of the schwann cell response to nerve injury. *Frontiers in Cellular Neuroscience*, *13*, 1–14. https://doi.org/10.3389/fncel.2019.00033

Jessen, K. R., Mirsky, R., & Lloyd, A. C. (2015). Schwann cells: Development and role in nerve repair. *Cold Spring Harbor Perspectives in Biology*, *7*(7), 1–15. https://doi.org/10.1101/cshperspect.a020487

Katsuno, Y., & Derynck, R. (2021). Epithelial plasticity, epithelial-mesenchymal transition, and the TGF-β family. *Developmental Cell*, *56*(6), 726–746.

Kawakami, K. (2004). Transgenesis and gene trap methods in zebrafish by using the Tol2 transposable element. *Methods in Cell Biology*, *77*, 201–22. https://doi.org/10.1016/s0091-679x(04)77011-9

Keatinge, M., Tsarouchas, T. M., Munir, T., Porter, N. J., Larraz, J., Gianni, D., Tsai, H.-H., Becker, C. G., Lyons, D. A., & Becker, T. (2021). CRISPR gRNA phenotypic screening in zebrafish reveals pro-regenerative genes in spinal cord injury. *PLoS Genetics*, *17*(4), 1–21. https://doi.org/10.1371/journal.pgen.1009515

Kim, J. S., Kim, J. G., Moon, M. Y., Jeon, C. Y., Won, H. Y., Kim, H. J., Jeon, Y.-J., Seo, J.-Y., Kim, J.-I., Kim, J., Lee, J.-Y., Kim, P.-H., & Park, J. B. (2006). Transforming growth factor-β1 regulates macrophage migration via RhoA. *Blood*, *108*(6), 1821–9. https://doi.org/10.1182/blood-2005-10-009191

Kimmel, C. B., Ballard, W. W., Kimmel, S. R., Ullmann, B., & Schilling, T. F. (1995). Stages of embryonic development of the zebrafish. *Developmental Dynamics*, *203*(3), 253–310. https://doi.org/10.1002/aja.1002030302

Kirby, B. B., Takada, N., Latimer, A. J., Shin, J., Carney, T. J., Kelsh, R. N., & Appel, B. (2006). In vivo time-lapse imaging shows dynamic oligodendrocyte progenitor behavior during zebrafish development. *Nature Neuroscience*, *9*(12), 1506–1511. https://doi.org/10.1038/nn1803

Kitisin, K., Saha, T., Blake, T., Golestaneh, N., Deng, M., Kim, C., Tang, Y., Shetty, K., Mishra, B., & Mishra, L. (2007). TGF-β Signaling in Development. *Science Signaling*, *2007*(399), 1–5. https://doi.org/10.1126/stke.3992007cm1

Kucenas, S. (2015). Perineurial glia. *Cold Spring Harbor Perspectives in Biology*, *7*(6), 1–14. https://doi.org/10.1101/cshperspect.a020511

Kucenas, S., Snell, H., & Appel, B. (2008). Nkx2.2a promotes specification and differentiation of a myelinating subset of oligodendrocyte lineage cells in zebrafish. *Neuron Glia Biology*, *4*(2), 71–81. https://doi.org/10.1017/S1740925X09990123

Kucenas, S., Takada, N., Park, H. C., Woodruff, E., Broadie, K., & Appel, B. (2008). CNS-derived glia ensheath peripheral nerves and mediate motor root development. *Nature Neuroscience*, *11*(2), 143–151. https://doi.org/10.1038/nn2025

Kwan, K. M., Fujimoto, E., Grabher, C., Mangum, B. D., Hardy, M. E., Campbell, D. S., Parant, J. M., Yost, H. J., Kanki, J. P., & Chien, C. B. (2007). The Tol2kit: A multisite gateway-based construction kit for Tol2 transposon transgenesis constructs, *236*(11), 3088–3099. *Developmental Dynamics*. https://doi.org/10.1002/dvdy.21343

Lai, S., Kumari, A., Liu, J., Zhang, Y., Zhang, W., Yen, K., & Xu, J. (2021). Chemical screening reveals Ronidazole is a superior prodrug to metronidazole for nitroreductase-induced cell ablation system in zebrafish larvae. *Journal of Genetics and Genomics*, *48*(12), 1081–1090. https://doi.org/10.1016/j.jgg.2021.07.015

Lenkowski, J. R., Qin, Z., Sifuentes, C. J., Thummel, R., Soto, C. M., Moens, C. B., & Raymond, P. A. (2013). Retinal regeneration in adult zebrafish requires regulation of TGFβ signaling. *Glia*, *61*(10), 1687–1697. https://doi.org/10.1002/glia.22549

Lewis, G. M., & Kucenas, S. (2013). Motor nerve transection and time-lapse imaging of glial cell behaviors in live zebrafish. *Journal of Visualized Experiments*, *76*, 1–6. https://doi.org/10.3791/50621

Lewis, G. M., & Kucenas, S. (2014). Perineurial glia are essential for motor axon regrowth following nerve injury. *The Journal of Neuroscience*, *34*(38), 12762–12777. https://doi.org/10.1523/jneurosci.1906-14.2014

Lopes, B., Sousa, P., Alvites, R., Branquinho, M., Sousa, A. C., Medonca, C., Atayde, L. M., Luís, A. L., Varejão, A. S., & Mauricio, A. C. (2022). Peripheral nerve injury treatments and advances: One health perspective - PubMed. *International Journal of Molecular Sciences*, *23*(2), 918.

Lyons, D. A., & Talbot, W. S. (2015). Glial cell development and function in zebrafish. *Cold Spring Harbor Perspectives in Biology*, *7*(2), 1–21. https://doi.org/10.1101/cshperspect.a020586

Marques, I., Lupi, E., & Mercader, N. (2019). Model systems for regeneration: zebrafish. *Development*, *146*(18), dev167692.

Meeker, N. D., Hutchinson, S. A., Ho, L., & Trede, N. S. (2007). Method for isolation of PCR-ready genomic DNA from zebrafish tissues. *BioTechniques*, *43*(5), 610–614. https://doi.org/10.2144/000112619

Menorca, R. M. G., Fussell, T. S., & Elfar, J. C. (2013). Nerve physiology. Mechanisms of injury and recovery. *Hand Clinics*, *29*, 317–330. https://doi.org/10.1016/j.hcl.2013.04.002

Min, Q., Parkinson, D. B., & Dun, X. P. (2021). Migrating Schwann cells direct axon regeneration within the peripheral nerve bridge. *Glia*, *69*, 235–254. https://doi.org/10.1002/glia.23892

Mokalled, M. H., Patra, C., Dickson, A. L., Endo, T., Stainier, D. Y. R., & Poss, K. D. (2016). Injury-induced *ctgfa* directs glial bridging and spinal cord regeneration in zebrafish. *Science*, *354*(6312), 630–634. https://doi.org/10.1126/science.aaf2679

Mokalled, M. H., & Poss, K. D. (2018). A regeneration toolkit. *Developmental Cell*, *47*, 267–280. https://doi.org/10.1016/j.devcel.2018.10.015

Morris, A. D., Lewis, G. M., & Kucenas, S. (2017). Perineurial glial plasticity and the role of TGF-β in the development of the blood–nerve barrier. *The Journal of Neuroscience*, *37*(18), 4790–4807. https://doi.org/10.1523/jneurosci.2875-16.2017

Mukherjee, D., Wagh, G., Mokalled, M. H., Kontarakis, Z., Dickson, A. L., Rayrikar, A., Günther, S., Poss, K. D., Stainier, D. Y. R., & Patra, C. (2021). Ccn2a is an injury-induced matricellular factor that promotes cardiac regeneration in zebrafish. *Development*, *148*(2), 1–16. https://doi.org/10.1242/dev.193219

Myers, P. Z., Eisen, J. S., & Westerfield, M. (1986). Development and axonal outgrowth of identified motoneurons in the zebrafish. *The Journal of neuroscience: The Official Journal of the Society for Neuroscience*, *6*(8), 2278–2289.

Nakamura, M., Yoshida, H., Moriyama, Y., Kawakita, I., Wlizla, M., Takebayashi-Suzuki, K., Horb, M. E., & Suzuki, A. (2021). TGF-β1 signaling is essential for tissue regeneration in the Xenopus tadpole tail. *Biochemical and Biophysical Research Communications*, *565*, 91–96.

Park, H. C., Mehta, A., Richardson, J. S., & Appel, B. (2002). olig2 is required for zebrafish primary motor neuron and oligodendrocyte development. *Developmental Biology*, *248*(2), 356–368. https://doi.org/10.1006/dbio.2002.0738

Parrinello, S., Napoli, I., Ribeiro, S., Digby, P. W., Fedorova, M., Parkinson, D. B., Doddrell, R. D. S., Nakayama, M., Adams, R. H., & Lloyd, A. C. (2010). EphB signaling directs peripheral nerve regeneration through Sox2-dependent Schwann cell sorting. *Cell*, *143*(1), 145–155. https://doi.org/10.1016/j.cell.2010.08.039

Pauls, S., Zecchin, E., Tiso, N., Bortolussi, M., & Argenton, F. (2007). Function and regulation of zebrafish nkx2.2a during development of

pancreatic islet and ducts. *Developmental Biology*, *304*(2), 875–890. https://doi.org/10.1016/j.ydbio.2007.01.024

Peltonen, S., Alanne, M., & Peltonen, J. (2013). Barriers of the peripheral nerve. *Tissue Barriers*, *1*(3), 1–7. https://doi.org/10.4161/tisb.24956

Popović, M., Bresjanac, M., & Sketelj, J. (1994). Regenerating axons enhance differentiation of perineurial-like cells involved in minifascicle formation in the injured peripheral nerve. *Journal of Neuropathology and Experimental Neurology*, *53*(6), 590–597. https://doi.org/10.1097/00005072-199411000-00006

Poss, K. D., Wilson, L. G., & Keating, M. T. (2002). Heart regeneration in zebrafish. *Science*, *298*(5601), 2188–2190. https://doi.org/10.1126/science.1077857

Rosenberg, A. F., Isaacman-Beck, J., Franzini-Armstrong, C., & Granato, M. (2014). Schwann cells and deleted in colorectal carcinoma direct regenerating motor axons towards their original path. *Journal of Neuroscience*, *34*(44), 14668–14681. https://doi.org/10.1523/JNEUROSCI.2007-14.2014

Rosenberg, A. F., Wolman, M. A., Franzini-Armstrong, C., & Granato, M. (2012). In vivo nerve-macrophage interactions following peripheral nerve injury. *The Journal of Neuroscience*, *32*(11), 3898–3909. https://doi.org/10.1523/jneurosci.5225-11.2012

Schira, J., Heinen, A., Poschmann, G., Ziegler, B., Hartung, H.-P., Stühler, K., & Küry, P. (2018). Secretome analysis of nerve repair mediating Schwann cells reveals Smad-dependent trophism. *The FASEB Journal*, *33*(4), 4703–4715. https://doi.org/10.1096/fj.201801799r

Schröder, J. M., May, R., & Weis, J. (1993). Perineurial cells are the first to traverse gaps of peripheral nerves in silicone tubes. *Clinical Neurology and Neurosurgery*, *95*, 78–83. https://doi.org/10.1016/0303-8467(93)90040-N

Sharma, P., Gupta, S., Chaudhary, M., Mitra, S., Chawla, B., Khursheed, M. A., Saran, N. K., & Ramachandran, R. (2020). Biphasic role of Tgf-β signaling during Müller glia reprogramming and retinal regeneration in zebrafish. *IScience*, *23*(2), 1–23. https://doi.org/10.1016/j.isci.2019.100817

Shi, W. C., Fang, Z. B., Li, L., & Luo, L. F. (2015). Using zebrafish as the model organism to understand organ regeneration. *Science China. Life Sciences*, *58*, 343–351. https://doi.org/10.1007/s11427-015-4838-z

Smith, C. J., Morris, A.D., Welsh, T.G., Kucenas, S., & Barres, B.A. (Eds.). (2014). Contact-mediated inhibition between oligodendrocyte progenitor cells and motor exit point Glia establishes the spinal cord transition zone. *PLoS Biol*. *12*(9), 1–15. https://doi.org/10.1371/journal.pbio.1001961

Sulaiman, W., & Nguyen, D. H. (2016). Transforming growth factor beta 1, a cytokine with regenerative functions. *Neural Regeneration Research*, *11*(10), 1549–1552. https://doi.org/10.4103/1673-5374.193223

Sun, Z., Jin, P., Tian, T., Gu, Y., Chen, Y. G., & Meng, A. (2006). Activation and roles of ALK4/ALK7-mediated maternal TGFβ signals in zebrafish embryo. *Biochemical and Biophysical Research Communications*, *345*(2), 694–703. https://doi.org/10.1016/j.bbrc.2006.04.148

Villegas, R., Martin, S. M., O'Donnell, K. C., Carrillo, S. A., Sagasti, A., & Allende, M. L. (2012). Dynamics of degeneration and regeneration in developing zebrafish peripheral axons reveals a requirement for extrinsic cell types. *Neural Development*, *7*(1), 1–14. https://doi.org/10.1186/1749-8104-7-19

Waller, A. (1850). XX. Experiments on the section of the glossopharyngeal and hypoglossal nerves of the frog, and observations of the alterations produced thereby in the structure of their primitive fibres. *Philosophical Transactions of the Royal Society of London*, *140*, 423–429. https://doi.org/10.1098/rstl.1850.0021

Webber, C., & Zochodne, D. (2010). The nerve regenerative microenvironment: Early behavior and partnership of axons and Schwann cells. *Experimental Neurology*, *223*, 51–59. https://doi.org/10.1016/j.expneurol.2009.05.037

Witzel, C., Rohde, C., & Brushart, T. M. (2005). Pathway sampling by regenerating peripheral axons. *The Journal of Comparative Neurology*, *485*(3), 183–190. https://doi.org/10.1002/cne.20436

Zaykov, V., & Chaqour, B. (2021). The CCN2/CTGF interactome: an approach to understanding the versatility of CCN2/CTGF molecular activities - PubMed. Retrieved October 14, 2021, from Journal of Cell Communication and Signaling website: https://pubmed.ncbi.nlm.nih.gov/34613590/

Zhang, S.-M., Wei, C.-Y., Wang, Q., Wang, L., Lu, L., & Qi, F.-Z. (2021). M2-polarized macrophages mediate wound healing by regulating connective tissue growth factor via AKT, ERK1/2, and STAT3 signaling pathways. *Molecular Biology Reports*, *48*(9), 6443–6456.

Zhu, Y., Crowley, S. C., Latimer, A. J., Lewis, G. M., Nash, R., & Kucenas, S. (2019). Migratory neural crest cells phagocytose dead cells in the developing nervous system. *Cell*, *179*(1), 74–89. https://doi.org/10.1016/j.cell.2019.08.001

Zochodne, D. W. (2012). The challenges and beauty of peripheral nerve regrowth. *Journal of the Peripheral Nervous System*, *17*, 1–18. https://doi.org/10.1111/j.1529-8027.2012.00378.x

SUPPORTING INFORMATION

Additional supporting information may be found in the online version of the article at the publisher's website.

How to cite this article: Arena, K. A., Zhu, Y., & Kucenas, S. (2022). Transforming growth factor-beta signaling modulates perineurial glial bridging following peripheral spinal motor nerve injury in zebrafish. *Glia*, *70*(10), 1826–1849. https://doi.org/10.1002/glia.24220